# TOROIDAL QUANTISATION APPROACH: A BOUNDARY-CURVATURE DERIVATION OF THE COSMOLOGICAL CONSTANT

#### Charles Emmanuel Levine

Independent Researcher

#### ABSTRACT

**Problem.** The physical origin of the cosmological constant  $\Lambda$  remains unsettled; in standard practice,  $\Lambda$  is inserted as a free parameter in Einstein's equations and tuned to data. **Method.** Develop a boundary–curvature framework on an embedded toroidal manifold. Motion on this surface follows brachistochrone (least–time) helical paths, so quantisation is performed *per radian*: the reduced Planck constant  $\hbar$  plays the central role and the  $2\pi$  factor associated with h does not appear. Entropy is evaluated via the Bekenstein–Hawking law, and a four–sector tripling rule for microstate amplification is enforced. One measured outer circumference  $c_0$  anchors the construction. The per–radian normalization is not an assumption: it is derived explicitly from the Einstein–Hilbert action with the Gibbons–Hawking–York (GHY) boundary term (Appendix E; see Sec. 10 for a concise summary and Sec. 11 for its connections to holography). **Result.** With  $r_h = c_0/(8\pi)$  and  $K = 1/r_h^2$ , the cross–sector coefficient  $\omega_{\text{mix}} = 7/15$ , together with the dimensionless bridge  $C_f$ , yields a closed, rational prediction:

$$\Lambda = \left(\frac{45927}{42050}\right) \times 10^{-52} \,\mathrm{m}^{-2} \approx 1.0922 \times 10^{-52} \,\mathrm{m}^{-2},$$

consistent with the 2025 consensus band  $(1.10\pm0.05)\times10^{-52}\,\mathrm{m^{-2}}$  and obtained without any adjustable empirical parameters.

Falsifiability and Scope. The framework defines three dimensionless invariants: (1) the per-radian offset  $1/(2\pi)$ , (2) the replication-invariant cross-sector ratio  $\omega_{\text{mix}} = 7/15$ , and (3) the slope--2 sensitivity  $\partial \Lambda/\partial c_0 = -2\Lambda/c_0$ . Its validity is explicitly contingent upon the Minimal-Closure Brachistochrone Toroid (MCBT) premise.

**Evidence Status.** This manuscript reports no direct physical measurements. Experimental validation remains *proposed* (Sec. C) and *simulated* (Appendices F and H) only.

#### **Keywords**

boundary—curvature law; brachistochrone closure; cross-sector mixing; entanglement—gravity crossover; holo-graphic entropy; microstate combinatorics; minimal-closure toroid; per-radian normalization; toroidal quantisation; cosmological constant.

#### Contents

1	Introduction	3
2	Definitions and Terminology	4
3	Assumptions and Scope	5
4	Closed Cycloid (Brachistochrone) and Cross-Sector Mixing Law	6
5	Microstate Growth and Cross-Sector Mixing Coefficient	8

b	Cosmological Constant — Canonical Curvature Route	8
7	Boundary Law and Inversion for $\hbar$ (Circumference–Based)	9
8	GR Conversions and Background Relations	9
9	Observational $\Lambda$ (For Comparison; not a fit)	10
10	Per-radian normalization at the boundary (summary)	10
11	Linkage to Holography and Quantum-Gravity Formulations	11
12	Positioning and Non-Equivalence to Competing Frameworks	11
13	Physical Interpretation of the Geometry	12
14	Dynamics, Stability, and Perturbations	12
15	FLRW Cosmology and Expansion History	13
16	Uncertainty Analysis	13
17	Comparison to Vacuum-Energy Approaches	13
18	Domain of Validity and Non-Circularity	13
19	Additional Observable Predictions	14
20	Conceptual Flow Diagram and Framework Summary	14
21	Comparison with Other Dark-Energy Frameworks	15
<b>22</b>	Microphysical Derivation of $c_0$ (Hypothesis: Entanglement–Gravity Crossover)	15
A	Symbol Glossary	17
В	Acronyms	17
$\mathbf{C}$	Experimental Roadmap	18
A	Worked Numeric Substitution for $\Lambda$ (Canonical Rational Form)	19
В	Scaling Factor $C_f$ (Derivation)	19
$\mathbf{C}$	Parametric Numeric Check for $\hbar$	20
D	Theorem-Level Derivation of the Microstate Rule (MCBT $\Rightarrow$ (1,1,3) $\Rightarrow$ $W(n) = 4 \cdot 3^n$ )	20
${f E}$	Per-radian normalization from the Einstein–Hilbert action	21
$\mathbf{F}$	Simulated Boundary–Curvature Experiment (Protocol; no physical data)	22
$\mathbf{G}$	Per-radian normalization from the Einstein–Hilbert boundary term (GHY route)	23
Н	Deterministic Simulation (Boundary–Curvature Sweep; verification only)	<b>2</b> 4
Ι	Microphysical Derivation of $c_0$ (Full Details)	25

#### 1 Introduction

Observations of the cosmic microwave background, distant supernovae, and large-scale structure consistently indicate the presence of a small but nonzero cosmological constant,  $\Lambda$ [Collaboration *et al.*(2020)Collaboration *et al.*(2025)Collaboration *et al.*, Collaboration *et al.*(2024)Collaboration *et al.*]. These analyses converge on values of order  $10^{-52}$  m<sup>-2</sup>, yet the physical origin of this term remains unsettled. In conventional treatments,  $\Lambda$  is introduced as a free parameter in Einstein's equations and tuned to observations. While successful phenomenologically, this approach provides no first-principles explanation for why  $\Lambda$  takes its observed value[Einstein(1917), Fritzsch(1984), Jordan(1955)].

This work develops a geometric and holographic alternative. The framework models spacetime dynamics on a toroidal surface, with motion advancing along brachistochrone-type (least-time) helical paths. Because these trajectories are intrinsically rotational, quantisation proceeds naturally on a per-radian basis, making the reduced Planck constant  $\hbar$  the fundamental unit. By contrast, a per-cycle formulation using h introduces an artificial  $2\pi$  factor. This link is made explicit by deriving the per-radian normalization from a recognised boundary term: (i) path-integral periodicity on  $S^1$  (Matsubara/KMS) and (ii) the  $2\pi$  that enters horizon/entropic gravity via Unruh temperature; see Sec. 10 (cf. [Verlinde(2011), Padmanabhan(2010)]).

The construction is holographic: bulk information is encoded on a codimension-1 boundary where state counting scales with area. Use standard labels (e.g., embedded toroidal manifold, holographic boundary) in equations; informal synonyms are confined to Sec. 2. Entropy uses the Bekenstein-Hawking area law[Bekenstein(1973), Hawking(1975)]; the microstate rule—four base sectors with tripling amplification—follows from minimal geodesic closure at fixed  $c_0$ .

Single-premise stance (MCBT). One premise is adopted, the Minimal-Closure Brachistochrone Toroid (MCBT). From this premise the microstate rule  $W(n) = 4 \cdot 3^n$  and sector weights (1, 1, 3) follow uniquely from it, where n denotes the fold or replication index in the microstate amplification (the number of tripling steps). No additional dynamical hypotheses are introduced.

Operational meaning of  $c_0$ . Throughout this work  $c_0$  denotes the single measured outer circumference that sets both curvature and boundary-area scales. It is not a cosmic-scale horizon length but a fixed microscopic closure scale. The minimal admissible circumference defining the toroidal quantisation boundary. Once  $c_0$  is fixed by observation or microphysical derivation, all downstream quantities—including  $r_h = c_0/(8\pi)$ ,  $\omega_{\rm mix}$ , and  $C_f$ —follow without further tuning. This constant establishes the geometric normalization for holographic state counting, all downstream quantities—including the curvature radius  $r_h = c_0/(8\pi)$ , the cross-sector coefficient  $\omega_{\rm mix}$ , and the scaling factor  $C_f$ —follow without further tuning.

Position in literature. Standard approaches treat  $\Lambda$  via (i) vacuum energy with regularization/renormalization choices, (ii) dynamical dark-energy fields (quintessence), (iii) modified-gravity terms, or (iv) holographic bounds. Vacuum-energy approaches tend to overestimate  $\Lambda$  by  $\sim 10^{120} [\text{Weinberg}(1989), \text{Padilla}(2015)]$ . Quintessence introduces scalar potentials with multiple free parameters tuned to match the expansion history[Copeland et al.(2006)Copeland, Sami, and Tsujikawa]. Modified-gravity theories alter the Einstein-Hilbert action with extra curvature terms, producing effective  $\Lambda$ -like contributions but facing strong solar-system and cosmological constraints[Verlinde(2011), Padmanabhan(2010)]. Generic holographic dark-energy (HDE) models tie  $\Lambda$  to area/entropy bounds using IR cutoffs[Cohen et al.(1999)Cohen, Kaplan, and Nelson, Li(2004), Wang et al.(2017)Wang, Wang, and Li]; recent post-DESI reassessments sharpen this landscape and still generally yield proportionalities rather than closed predictions[Li et al.(2025)Li, Li, Du, Wu, Feng, Zhang, and Zhang, Samaddar et al.(2024)Samaddar et al., Luciano et al.(2025)Luciano, Paliathanasis, and Saridakis]. Recent entropic/thermodynamic gravity routes (e.g., [Bianconi(2025), Alonso-Serrano and Liska(2025)]) also motivate boundary-based constructions but do not produce a closed rational  $\Lambda$ .

#### How this differs from HDE (explicit).

- Closed-form value, not a proportionality:  $\Lambda = \left(\frac{45927}{42050}\right) \times 10^{-52} \,\mathrm{m}^{-2}$ .
- Fixed curvature scale:  $r_h = c_0/(8\pi)$ ; no IR cutoff or horizon-choice tuning
- Integer structure: (1,1,3) sectoring and  $\omega_{\text{mix}} = 7/15$  are counting identities from closure geometry.

- Dimensionless bridge:  $C_f$  reconciles per-radian counting with Planck-unit  $S_{BH}$ ; it is not a fit parameter.
- Concrete tests: per-radian offset  $1/(2\pi)$ , replication-invariant  $\omega_{\text{mix}}$ , and slope -2 sensitivity to  $c_0$ .

Motivation for Minimal-Closure Brachistochrone Toroid (MCBT)

The Minimal-Closure Brachistochrone Toroid (MCBT) premise selects, among admissible closed boundary flows, the least-circumference helical geodesic that preserves single-valued boundary mapping and arch periodicity. It mirrors (i) brachistochrone/tautochrone optimality for rotational motion[Tikhomirov(1990)] and (ii) Euclidean near-horizon regularity where the angular variable is fundamental. In this setting the torus arises as the minimally self-consistent compact surface supporting a single global angular clock and a meridional step, with closure enforcing an integer sector partition. This geometric + variational selection does not introduce a new force law; its falsifiable outputs are the per-radian offset  $1/(2\pi)$ , the replication-invariant leakage  $\omega_{\rm mix} = 7/15$ , and the slope -2 sensitivity  $\partial \Lambda/\partial c_0$ .

Why a torus? A torus is the simplest closed surface that supports two independent periodic directions: one angular coordinate around the "hole" and one around the "tube." In the boundary–curvature setting, the global angular coordinate provides a natural clock for per-radian quantisation, while the meridional coordinate tracks the helical advance. The requirement that the geodesic returns to its starting point without self-intersection singles out a torus over other compact surfaces (e.g., a sphere lacks a second noncontractible loop). The Minimal-Closure premise enforces that this closed geodesic has the least possible circumference among all admissible brachistochrone paths, mirroring familiar extremal principles such as least-action or least-time. Thus the choice of an embedded toroidal geometry is not arbitrary but follows from seeking a minimal self-consistent configuration for rotational motion.

On parameter count. Once  $c_0$  is specified, the construction fixes  $\Lambda$  without any additional knobs. Competing classes typically require at least two tuned quantities—for example, an IR cutoff scale and a dimensionless coefficient in holographic dark-energy models, or potential parameters in quintessence. In contrast,  $r_h = c_0/(8\pi)$ ,  $\omega_{\text{mix}} = 7/15$ , and the bridging factor  $C_f$  are fixed by boundary closure and per-radian counting; there remain zero fit parameters beyond the circumference.

Roadmap of the Paper. For clarity, briefly outlined is how the argument proceeds. Section 2 collects definitions and establishes notation. Section 4 constructs the closed cycloid on the unwrapped boundary and derives the (1,1,3) partition from the Minimal-Closure Brachistochrone Toroid (MCBT) premise. Section 5 uses this partition to compute the microstate growth law  $W(n) = 4 \cdot 3^n$  and the cross-sector mixing coefficient  $\omega_{\text{mix}} = 7/15$ . Section 6 combines the curvature scale  $r_h = c_0/(8\pi)$  with these combinatorial factors and a dimensionless bridge  $C_f$  to obtain a closed expression for the cosmological constant. Section 7 checks consistency by matching the microstate entropy to the Bekenstein–Hawking area law and inverting for  $\hbar$ . Later sections place the result in the context of holography and quantum gravity (Section 11), contrast it with competing frameworks (Section 12), explore a microphysical derivation of  $c_0$  (Section 22), and discuss falsifiability, experimental proposals, and next steps. A summary of assumptions and the domain of validity is provided in Section 3.

# 2 Definitions and Terminology

*Purpose*. Consolidates symbols and terms used throughout. Informal synonyms appear here only and are *not* used in equations; standard terms follow differential-geometry usage.

Units and Conventions

- per-radian normalization: quantisation is counted in units of  $\hbar$  (per radian). Per-cycle quantities use  $h = 2\pi\hbar$  only by contrast.
- GR and constants: Standard GR sign conventions; c (speed of light), G (Newton's constant),  $k_B$  (Boltzmann's constant).
- Curvature convention:  $K := 1/r_h^2$  with  $r_h = c_0/(8\pi)$ .

#### Geometric Quantities

- Outer circumference  $c_0$ : The single measured length that anchors both curvature and boundary area scales. Fixed here at  $c_0 = \left(\frac{29}{27}\right) \times 10^{-35}$  m.
- Horizon curvature radius  $\mathbf{r_h}$ :  $r_h := c_0/(8\pi)$ ; sets the curvature scale  $K = 1/r_h^2$ . Used in the  $\Lambda$  route.
- Horn-torus radius parameter R:  $R := c_0/(4\pi)$ . This is the radius implied by taking the outer circumference as  $2\pi (2R)$ ; it is used only in the entropy-extremum context and does not enter the  $\Lambda$  derivation.
- Entropy-boundary radius  $\mathbf{r}_*$ :  $r_* := c_0/(8\pi)$ ; used in  $A = \alpha \pi r_*^2$  for  $S_{\rm BH}$ , where  $\alpha$  is a dimensionless geometric factor (for example,  $\alpha = 4$  for a spherical horizon).
- Toroidal quantisation surface (mainstream): Closed surface on which helical trajectories advance.
- Unwrapped boundary periods:  $(c_0, c_0/2)$  defining the rectangular parameter domain used for cycloid closure.
- Bridging factor  $C_f$ : A dimensionless factor that reconciles per-radian microstate counting with the Planck-unit Bekenstein-Hawking entropy. Once the outer circumference  $c_0$  is fixed, the bridge  $C_f$  has a specific value—derived in Sec. 6 as  $C_f = \frac{27}{160\pi^2} \times 10^{-122}$ —and is not an adjustable parameter.

Cycloid / Brachistochrone Construction

- Cycloid arch scale  $\mathbf{r_b}$ :  $x(\theta) = r_b(\theta \sin \theta)$ ,  $y(\theta) = r_b(1 \cos \theta)$  for  $\theta \in [0, 2\pi]$ ; pitch  $P = 2\pi r_b$ , arch length  $L_{\rm arch} = 8r_b$ .
- 12-arch closure: Enforce  $12P = c_0 \Rightarrow r_b = c_0/(24\pi)$ ; meridional steps  $\Delta v_j = \frac{w_j}{40}c_0$  with weights  $w = (1, 1, 3) \times 4$ , giving  $\sum_{j=1}^{12} \Delta v_j = c_0/2$  and fixing  $r_h$ .
- Per-arch scaling  $\beta_i$ :  $\beta_i := \Delta v_i / L_{\text{arch}} = (3\pi/40) w_i$ ; sets the (1:3) sectoring in each period.

Premise and Logical Status of the Microstate Rule

**Premise (MCBT).** A toroidal quantisation surface whose closed geodesic flow is a 12-arch brachistochrone closure at the smallest admissible circumference, preserving single-valued boundary mapping and arch periodicity. Claim (premise $\Rightarrow$ rule). Given MCBT, the phase-advance partition of one period is constrained to the integer ratio (1,1,3) (replicated), inducing a four-set Markov partition with tripling map. Hence  $W(n) = 4 \cdot 3^n$  is exact under MCBT. The cross-sector mixing coefficient is the counting identity

$$\omega_{\text{mix}} = \frac{1}{3} \frac{\sum_{i < j} w_i w_j}{W_{\text{tot}}} = \frac{7}{15},$$

where  $W_{\text{tot}} = \sum_{i} w_{i}$  denotes the total sector weight and should not be confused with the microstate multiplicity W(n). Here "replication invariance" refers to repeating the (1,1,3) block across the twelve arches (concatenating identical triples), which leaves  $\omega_{\text{mix}}$  unchanged; scaling each weight by a common factor k alters the ratio because the quadratic numerator and the linear denominator scale differently.

#### 3 Assumptions and Scope

**Key assumptions.** The derivation rests on the following foundational assumptions:

- 1. **Toroidal quantisation surface.** The holographic boundary is a closed two–surface topologically a torus, providing a single global angular coordinate and a meridional direction. Motion on this surface follows a brachistochrone (least–time) helical geodesic.
- 2. Minimal—Closure Brachistochrone Toroid (MCBT). Among admissible closed helical flows, the path with the smallest admissible circumference that preserves single—valued boundary mapping and arch periodicity is selected. This is the single premise adopted in this work.
- 3. **Per-radian normalization.** quantisation is counted per radian, making the reduced Planck constant  $\hbar$  the fundamental unit. This follows from Euclidean regularity of the Einstein–Hilbert + GHY action on a cylindrical neighborhood of a horizon (Sec. 10 and Appendix E).

- 4. Entropy law and General Relativity. The combinatorial microstate entropy is equated to the Bekenstein–Hawking entropy  $S_{\rm BH} = A/(4G\hbar)$ . Standard General Relativity with the Einstein–Hilbert action and its Gibbons–Hawking–York boundary term is assumed; no modifications or extra curvature terms enter. Because the construction rests on the standard Einstein–Hilbert action with the canonical boundary term, Lorentz invariance and general covariance are preserved; the toroidal geometry is a topological choice and does not introduce symmetry breaking.
- 5. Microphysical input  $c_0$ . A single measured outer circumference  $c_0$  sets the curvature and boundary–area scales. It is treated as a fundamental microphysical constant to be determined by experiment or by quantum–field–theoretic calculation (Sec. 22). Once  $c_0$  is fixed, all downstream quantities—such as  $r_h = c_0/(8\pi)$ ,  $\omega_{\text{mix}}$ , and  $C_f$ —follow without further tuning.
- 6. Single winding. The winding number m of the closed path around the major direction is unity. Higher windings would introduce an unconstrained integer and spoil the matching between the microstate entropy and the area law (Sec. 4).

Scope and limitations. Within the above premises, this framework derives the magnitude of the cosmological constant as a closed rational number. It does not address the quantum vacuum energy divergence in quantum field theory, nor does it modify the dynamics of General Relativity. The model operates within the standard  $\Lambda$ CDM cosmological paradigm: no alternative dark–energy component or modified gravity is introduced beyond the derivation of  $\Lambda$ . Relaxing the MCBT premise—such as permitting multiple windings, altering the topology of the quantisation surface, or modifying the entropy law—changes the integer partition and therefore alters  $\omega_{\text{mix}}$  and  $\Lambda$ . The results are thus contingent on MCBT. Furthermore, this work reports no direct physical measurements; all empirical comparisons rely on existing cosmological data or on simulations and proposed experiments (Sec. C).

# 4 Closed Cycloid (Brachistochrone) and Cross-Sector Mixing Law

One cycloid arch (arch boundary to arch boundary) with scale  $r_b > 0$ :

$$x(\theta) = r_b(\theta - \sin \theta), \quad y(\theta) = r_b(1 - \cos \theta), \quad \theta \in [0, 2\pi].$$

Pitch and arch length:

$$P = 2\pi r_b, \qquad L_{\rm arch} = 8 r_b.$$

Minimal-Closure Principle (MCBT). Among admissible toroidal brachistochrone closures, select the least-circumference closure that preserves single-valued boundary mapping and arch periodicity. This selection quantizes meridional steps into the (1,1,3) staircase and fixes sector-mixing combinatorics; repeating the (1,1,3) block across the 12 arches leaves  $\omega_{\text{mix}}$  invariant, whereas uniformly scaling the entries does not.

**Local definitions.** Winding number m denotes the integer number of equatorial traversals in a closed loop. Brachistochrone closure length  $L_{\text{brach}}$  denotes the total length of the closed cycloidal path on the boundary.

Closure on the holographic boundary. Unwrap to a rectangle with periods  $(c_0, \frac{c_0}{2})$ . Choose 12 arches so  $12P = c_0 \Rightarrow r_b = \frac{c_0}{24\pi}$ . Impose the meridional advances:

$$\Delta v_j = \frac{w_j}{40} c_0, \qquad w = (1, 1, 3) \times 4, \qquad \sum_{j=1}^{12} \Delta v_j = \frac{c_0}{2}.$$

The horn torus radius from the entropy extremum is  $R = c_0/(4\pi)$ . For curvature used in the  $\Lambda$  route, use  $r_h = c_0/(8\pi)$ .

Per-arch scaling  $\beta_j = \Delta v_j / L_{\rm arch} = (3\pi/40) w_j$  yields the exact closed path.

Canonical Closure Constraint

On the unwrapped rectangle with periods  $(c_0, c_0/2)$ , a closed brachistochrone path may wind  $m \in \mathbb{Z}_{>0}$  times around the equator, giving

$$L_{\text{brach}} = m c_0.$$

The 12-arch construction enforces  $P=2\pi r_b,\,12P=c_0,\,$  and  $\sum_{j=1}^{12}\Delta v_j=c_0/2$  (Sec. 4).

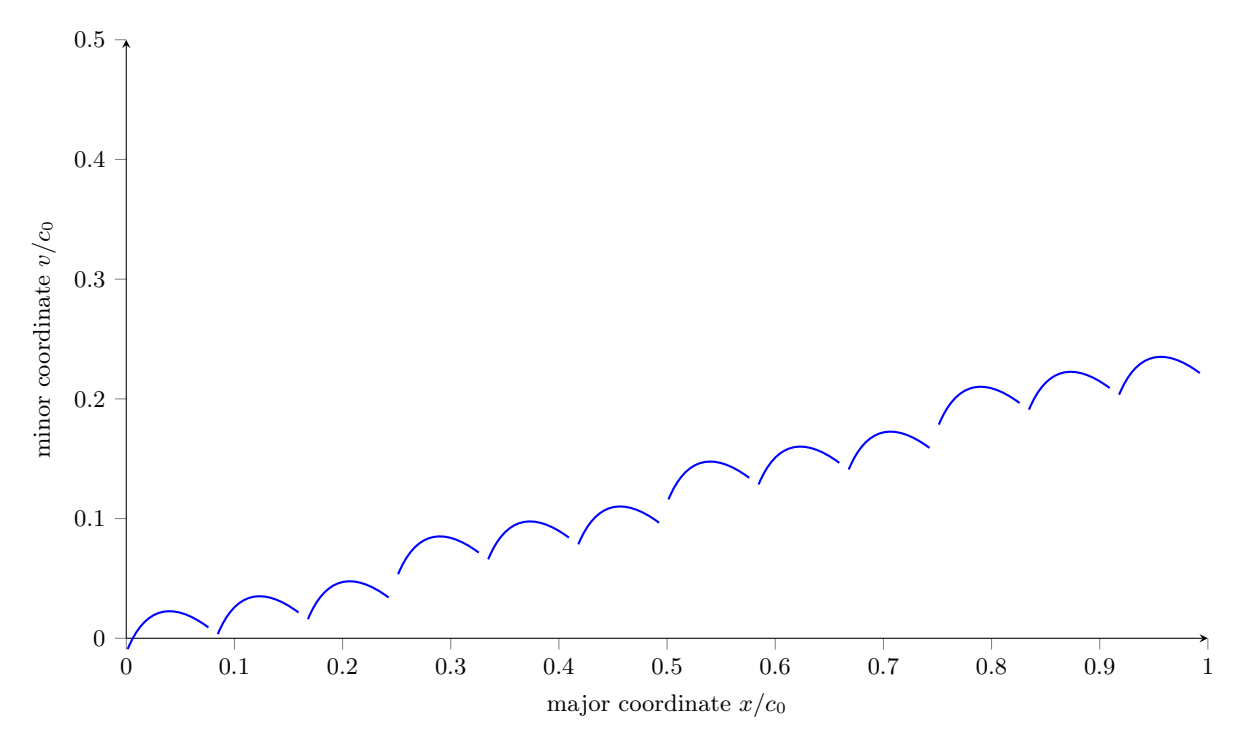


Figure 1: Unwrapped 12-arch pattern on the holographic boundary with continuous meridional advance. The monotonic rise of  $v/c_0$  across the twelve arches illustrates how the brachistochrone advances in the minor direction while wrapping around the major coordinate, confirming the continuous helical closure.

Entropy matching (necessity of m=1). On the geometric side, the Bekenstein-Hawking entropy with  $r_* = c_0/(8\pi)$  scales quadratically in  $c_0$ :

$$S_{\rm BH} = \frac{k_B c^3}{4G\hbar} \, \alpha \pi r_*^2 \, \propto \, c_0^2 \quad ({\rm Sec.} \, \, 7). \label{eq:SBH}$$

On the combinatorial side, the microstate rule yields

$$S_{\text{micro}}(m) = k_B \ln(W(n)^m) = m k_B (\ln 4 + n \ln 3) \propto m$$
 (Secs. 4, 7).

Equality  $S_{\rm BH} = S_{\rm micro}$  without introducing an extra tunable parameter is therefore possible only at the minimal nontrivial winding m = 1; any m > 1 injects an unconstrained integer not mirrored by the geometric term and breaks canonical consistency.

Result and corollary. Hence the entropy law enforces the minimal closure

$$L_{\text{brach}} = c_0,$$

i.e., a 1:1 ratio of closure length to outer circumference. As a corollary, the pulse count per cycle is strictly integer and fixed by this closure; discreteness is derived rather than assumed. The curvature scale  $r_h = c_0/(8\pi)$  used in Sec. 6 is thus fixed by closure, not chosen.

Section summary. In this section, the Minimal-Closure Brachistochrone Toroid (MCBT) premise is imposed on the unwrapped boundary. It was shown that a 12-arch closure forces a unique (1,1,3) staircase of meridional advances and fixes the curvature scale  $r_h = c_0/(8\pi)$ . These geometric constraints provide the foundation for the microstate growth law and the cosmological constant computation developed in the following sections.

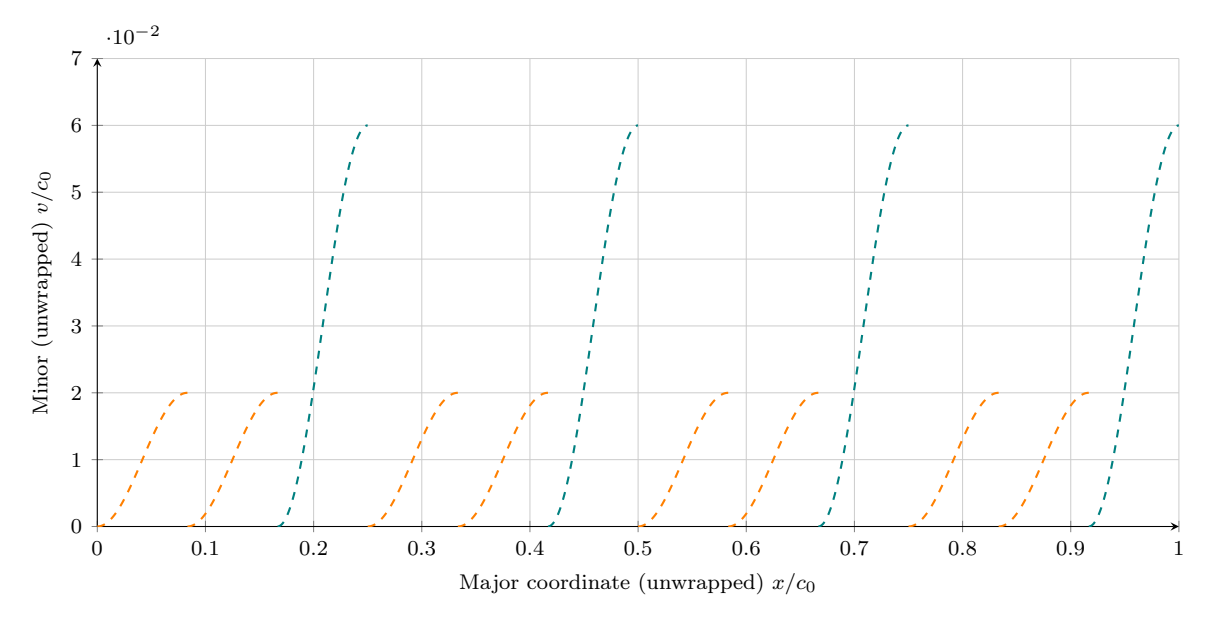


Figure 2: Schematic enforcing the Minimal-Closure Brachistochrone Toroid (MCBT): four repetitions of the meridional-advance pattern (1,1,3) across 12 arches. Any other integer partition would break closure; the (1,1,3) triple is the unique minimal block producing a closed path.

# 5 Microstate Growth and Cross-Sector Mixing Coefficient

**Derivation under MCBT.** The 12-arch brachistochrone closure forces a four-sector partition with a tripling return map  $T(\vartheta) = 3\vartheta \pmod{2\pi}$ . Therefore

$$W(n) = 4 \cdot 3^n$$
 (exact under MCBT).

Combinatorial entropy:  $S_{\text{micro}} = k_B \ln W(n)$  (see Sec. 7).

Cross-Sector Mixing (counting identity). For weights (1,1,3) with total  $W_{\text{tot}} = 5$ ,

$$\omega_{\text{mix}} = \frac{\frac{1}{3} \sum_{i < j} w_i w_j}{W_{\text{tot}}} = \frac{7}{15}.$$

In this notation  $W_{\text{tot}} = \sum_i w_i$  denotes the total sector weight, not the microstate multiplicity W(n). Replication invariance means that repeating the (1,1,3) triple across additional blocks (concatenating identical triples) leaves  $\omega_{\text{mix}}$  unchanged; uniform scaling of the weights does not preserve this ratio.

#### 6 Cosmological Constant — Canonical Curvature Route

Using the curvature radius  $r_h = c_0/(8\pi)$  and  $K = (8\pi/c_0)^2$ ,

$$\Lambda = \frac{7}{60} K C_f$$
 with  $K = \left(\frac{8\pi}{c_0}\right)^2$ ,  $C_f = \frac{27}{160\pi^2} \times 10^{-122}$ .

No tuned parameters enter once  $c_0$  is fixed;  $C_f$  is a dimensionless bridge forced by per-radian counting and Planck-unit  $S_{BH}$ , not an empirical knob.

Sensitivity form (for scans in  $c_0$ ). With  $K = (8\pi/c_0)^2$ ,

$$\Lambda(c_0) = \frac{112}{15} \, \frac{\pi^2}{c_0^2} \, C_f, \qquad \frac{\partial \Lambda}{\partial c_0} = -2 \, \frac{\Lambda}{c_0}. \label{eq:lambda}$$

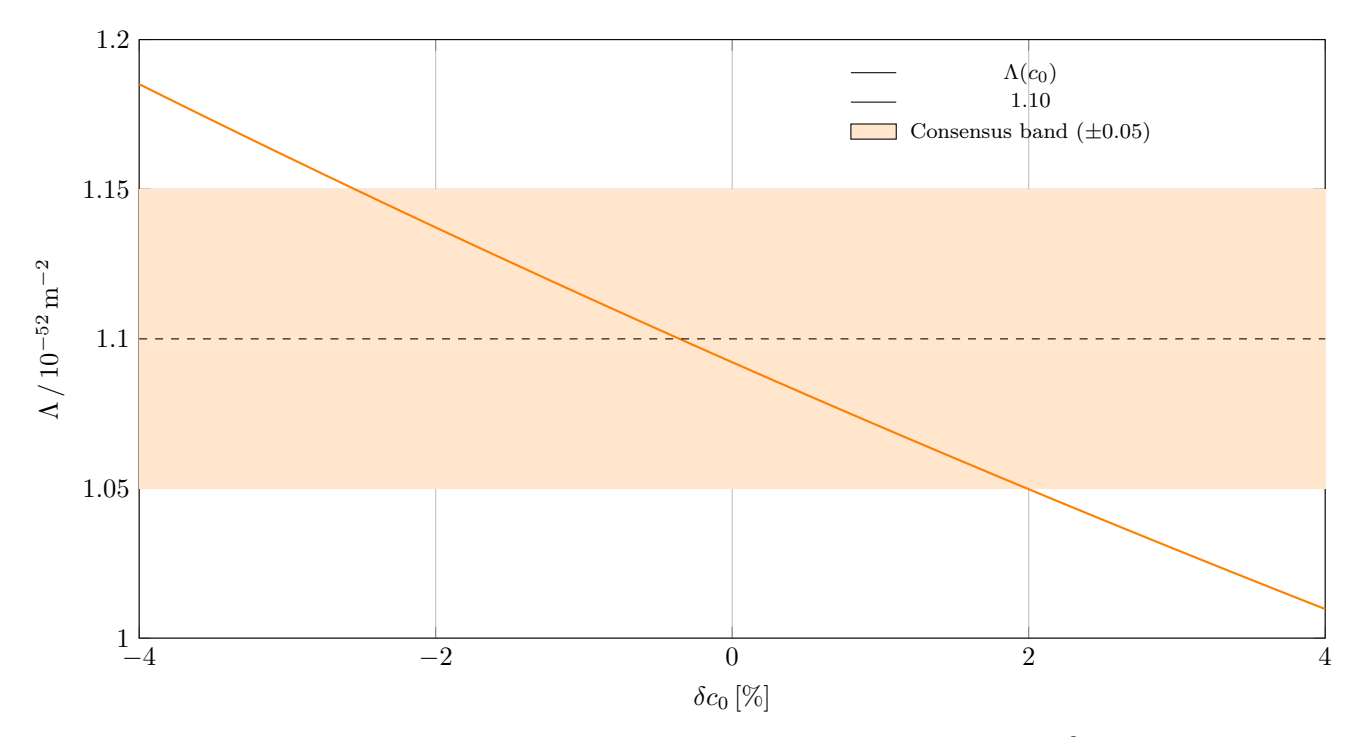


Figure 3: Sensitivity of  $\Lambda$  (units: m<sup>-2</sup>) to small fractional changes in  $c_0$  using  $\Lambda(c_0) = \frac{112}{15} \frac{\pi^2}{c_0^2} C_f$  with  $C_f = \frac{27}{160\pi^2} \times 10^{-122}$ . Solid line:  $\Lambda(c_0)$ . Dashed:  $1.10 \times 10^{-52} \,\mathrm{m}^{-2}$ . Shaded: observational consensus  $(1.10 \pm 0.05) \times 10^{-52} \,\mathrm{m}^{-2}$  (sources: [Collaboration *et al.*(2020)Collaboration *et al.*, Collaboration *et al.*(2024)Collaboration *et al.*]).

# 7 Boundary Law and Inversion for h (Circumference–Based)

For a circumference–based horizon, the effective boundary area is

$$A = \alpha \pi r_*^2, \qquad r_* := \frac{c_0}{8\pi}.$$

Here  $\alpha$  is a dimensionless geometric factor that encodes the shape of the boundary; for example,  $\alpha=4$  for a spherical horizon. In the toroidal construction, its precise value does not affect the final  $\Lambda$  prediction because it cancels out in the inversion for  $\hbar$ . Microstate entropy:

$$S_{\text{micro}} = k_B (\ln 4 + n \ln 3),$$

Bekenstein-Hawking entropy:

$$S_{\rm BH} = \frac{k_B c^3 A}{4G\hbar}.$$

Equating  $S_{\rm BH} = S_{\rm micro}$  gives

$$\hbar = \frac{c^3 \, \alpha \, c_0^2}{256 \, \pi \, G(\ln 4 + n \ln 3)}$$

which reproduces the correct order of magnitude for typical  $(\alpha, n)$  and serves as a consistency check.

# 8 GR Conversions and Background Relations

$$\rho_{\Lambda} = \frac{\Lambda c^2}{8\pi G}, \qquad \epsilon_{\Lambda} = \frac{\Lambda c^4}{8\pi G}, \qquad p_{\Lambda} = -\epsilon_{\Lambda}, \qquad \Lambda = \frac{3\,\Omega_{\Lambda} H_0^2}{c^2}.$$

Here,  $\Omega_{\Lambda}$  and  $H_0$  are defined in Appendix A.

# 9 Observational $\Lambda$ (For Comparison; not a fit)

$$\begin{split} & \Lambda_{\rm Planck~2018} \approx 1.09 \times 10^{-52}~{\rm m}^{-2}, \\ & \Lambda_{\rm DESI~Y1+}_{\rm Planck+ACT} \approx 1.12 \times 10^{-52}~{\rm m}^{-2}, \\ & \Lambda_{\rm DESI~Y1~BAO+}_{\rm BBN+CMB~\theta^*} \approx 1.16 \times 10^{-52}~{\rm m}^{-2}, \\ & \Lambda_{\rm ACT~DR6+}_{\rm Planck+DESI~Y1} \approx 1.14 \times 10^{-52}~{\rm m}^{-2}, \\ & \Lambda_{\rm Consensus} \approx (1.10 \pm 0.05) \times 10^{-52}~{\rm m}^{-2}. \end{split}$$

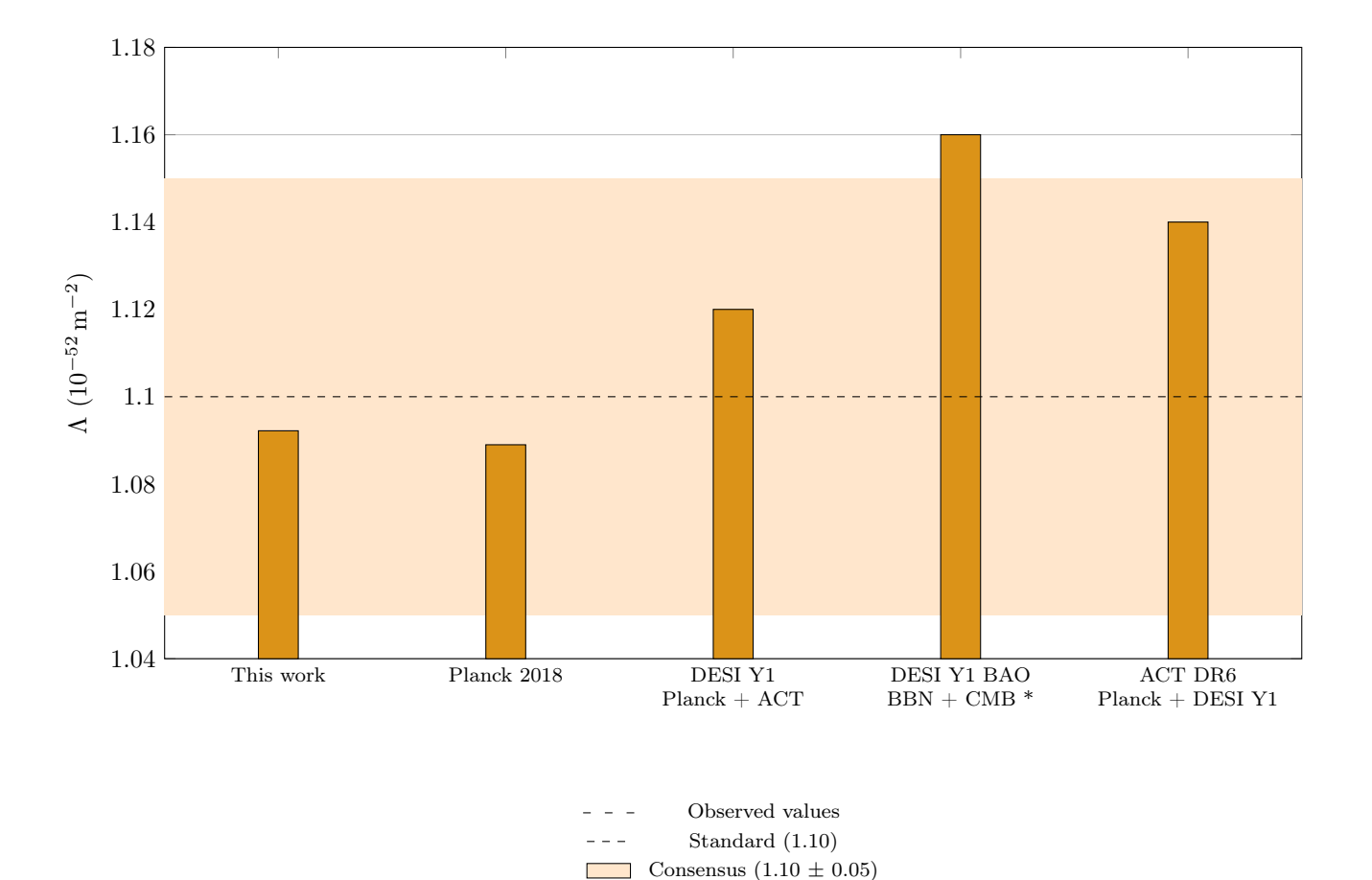


Figure 4: Comparison of  $\Lambda$  with recent cosmology datasets (all values in  $10^{-52} \,\mathrm{m}^{-2}$ ). Bars use dimensionless values shown in the original analysis. Shaded band and dashed line indicate the observational consensus (1.10  $\pm$  0.05) as in the reference figure.

# 10 Per-radian normalization at the boundary (summary)

The Euclidean GHY boundary term on a small cylindrical neighborhood of a nonextremal horizon yields

$$I_{\partial} = \frac{1}{8\pi G} \int_{\partial \mathcal{M}} K \sqrt{h} \, d^3 x \xrightarrow{\beta \kappa = 2\pi} \frac{A}{4G},$$

where  $\beta$  is the Euclidean period and  $\kappa$  the surface gravity. Writing the angular coordinate as  $\varphi := \kappa \tau \in [0, 2\pi)$  gives an action per unit angle

$$\frac{dI_{\partial}}{d\varphi} = \pm \frac{A}{8\pi G}.$$

Sign conventions for the Euclidean action differ by boundary orientation; the  $2\pi$  periodicity and per-radian normalization are invariant under either choice.

Hence quantisation is naturally per radian (unit  $\hbar$ ), with the operational offset  $f/\omega = 1/(2\pi)$  (boundary circle  $S^1$ ). Full derivations are provided in Appendix G (GHY route) and Appendix E (Einstein–Hilbert + GHY).

# 11 Linkage to Holography and Quantum-Gravity Formulations

Noether-charge / Wald entropy (GR side). On any bifurcate Killing horizon, the gravitational entropy equals the Noether charge [Wald (1993), Iyer and Wald (1994)]:

$$S_{ ext{Wald}} = rac{1}{T_{ ext{H}}} \int_{\mathcal{H}} Q[\xi] = rac{A}{4G\hbar} \, k_B,$$

with  $Q[\xi]$  the Noether 2-form for the horizon-generating Killing field  $\xi$  and  $T_{\rm H} = \hbar \kappa/(2\pi k_B)$  the Hawking temperature. The GHY derivation (Appendix G) reproduces the same  $2\pi$  via Euclidean regularity ( $\beta \kappa = 2\pi$ ), fixing the *per-radian* normalization ( $\hbar$ ) at the boundary. Hence the area law used in Sec. 7 is the Wald/Iyer-Wald entropy in the minimal GR setting.

Entanglement first law  $\Rightarrow$  Einstein equations (QFT side). For small perturbations of a ball-shaped region in the vacuum of a QFT, the entanglement first law  $\delta S = \delta \langle H_{\text{mod}} \rangle$  together with the modular Hamiltonian of the Rindler wedge implies the linearized Einstein equations when gravity is dynamical[Jacobson(1995), Faulkner et al.(2013)Faulkner, Lewkowycz, and Maldacena, Lashkari et al.(2014)Lashkari, McDermott, and Van Raamsdonk]:

$$\delta S_{\rm ent} = \frac{2\pi}{\hbar} \int_{\Sigma} \zeta^{\mu} T_{\mu\nu} d\Sigma^{\nu} \quad \Longleftrightarrow \quad \delta G_{\mu\nu} + \Lambda \, \delta g_{\mu\nu} = 8\pi G \, \delta T_{\mu\nu}.$$

This construction uses the same Rindler/KMS  $2\pi$  (Sec. 10) and treats the boundary counting per radian; the dimensionless bridge  $C_f$  reconciles this counting with Planck-unit  $S_{\rm BH}$  without introducing tunable IR cutoffs. Thus the microstate rule feeds into the same entanglement–gravity channel that underlies entropic derivations of field equations.

Ryu-Takayanagi / Hubeny-Rangamani-Takayanagi (RT/HRT) area law (AdS/CFT side). In holographic settings, boundary entanglement entropy equals the (extremal) area in Planck units[Ryu and Takayanagi(2006), Hubeny et al.(2007)Hubeny, Rangamani, and Takayanagi]:

$$S_{\rm EE} = rac{{
m Area}(\gamma_A)}{4G_N\hbar} \, k_B.$$

Although this geometry is not assumed AdS, the area-proportional entropy with the same  $1/(4G\hbar)$  coefficient is shared. Making no use of AdS curvature or an IR cutoff; instead, the curvature scale  $r_h = c_0/(8\pi)$  is fixed by cycloid closure (Sec. 4), and  $\Lambda$  follows rationally (Sec. 6). This positions the framework as compatible with RT/HRT's area-law normalization while remaining agnostic to bulk asymptotics.

Kubo-Martin-Schwinger (KMS) / Unruh and RT/HRT—consistency only. The same topological  $2\pi$  from KMS/Unruh underlies Wald entropy and RT/HRT area laws. The derivation of the factor is here; see Appendix E. This use is limited to consistency of the area coefficient  $1/(4G\hbar)$  and the per-radian normalization.

#### 12 Positioning and Non-Equivalence to Competing Frameworks

Non-equivalence criteria (concise).

- Closed rational prediction: This work yields a specific rational  $\Lambda$ , not a proportionality with a tunable IR scale (contrast: HDE).
- Fixed curvature scale:  $r_h = c_0/(8\pi)$  is fixed by boundary closure; no event-horizon/future-horizon choice (contrast: HDE, cutoff models).
- Integer combinatorics: (1,1,3) sectoring and  $\omega_{\text{mix}} = 7/15$  arise from closure kinematics; not available in vacuum-energy regularization or quintessence.
- No fit parameters:  $C_f$  is dimensionless bridging under per-radian counting, not an empirical knob.

Parameter count (concise contrast). Standard HDE/quintessence frameworks typically require  $\geq 2$  tuned quantities (e.g., horizon/IR cutoff choice plus a dimensionless coefficient; or potential parameters) to match  $\Lambda$ . The present construction fixes  $r_h = c_0/(8\pi)$ ,  $\omega_{\text{mix}} = 7/15$ , and the bridging factor  $C_f$  by boundary closure and per-radian counting, leaving zero fit parameters once  $c_0$  is fixed. This quantitative contrast explains why the result is a closed rational value rather than a proportionality.

Novelty vs. Precedent. While the present construction shares broad motivation with entropic and holographic gravity programs, it is not a variant of them. Standard entropic approaches (e.g. Verlinde, Padmanabhan) treat gravity as emergent from entropy gradients but do not derive a closed prediction for  $\Lambda$ . Generic HDE models enforce area-scaling bounds and introduce IR cutoffs, yielding proportionalities that depend on horizon choices. By contrast, the present framework produces a *specific rational fraction* for  $\Lambda$ ,

$$\Lambda = \frac{45927}{42050} \times 10^{-52} \,\mathrm{m}^{-2},$$

fixed uniquely by the minimal-closure brachistochrone toroid (MCBT) premise. The integer partition (1,1,3) and the cross-sector coefficient  $\omega_{\text{mix}} = 7/15$  arise as counting identities from closure geometry and cannot be tuned. The bridging factor  $C_f = \frac{27}{160\pi^2} \times 10^{-122}$  is dimensionless and forced by per-radian versus per-cycle counting, not a free knob. Thus, the novelty lies in the theorem-level derivation: once  $c_0$  is fixed, all outputs follow with no additional assumptions. This places the approach in a distinct category—boundary–curvature quantisation with integer-structure falsifiability—rather than an extension of existing entropic or holographic programs.

Falsifiable invariants (summary)

Three dimensionless handles enable verification:

- Per-radian offset:  $f/\omega = 1/(2\pi) \pm 2 \times 10^{-3}$ .
- Replication-invariant mixing:  $\omega_{\text{mix}} = 7/15 \pm 0.01$  under (k, k, 3k) scaling.
- Curvature sensitivity:  $d \ln \Lambda / d \ln c_0 = -2 \pm 0.05$  for  $|\Delta c_0/c_0| \le 2\%$ , with  $R^2 > 0.98$  in deterministic sweeps.

See Appendices F and H for experimental protocols and deterministic sweeps.

# 13 Physical Interpretation of the Geometry

The toroidal quantisation surface used throughout this work is not an abstract mathematical artifice; it has a concrete geometric meaning within general relativity. A torus supports two independent non-contractible loops, and the Minimal-Closure Brachistochrone Toroid (MCBT) premise selects the closed geodesic on this surface with minimal circumference. Physically, such a surface can be thought of as the boundary of a compact region where quantum degrees of freedom live. The major cycle encodes a global angular "clock," while the minor cycle encodes the helical advance of the brachistochrone path. Because the torus admits a single global angular coordinate and a meridional direction, the boundary plays the role of a holographic screen on which bulk information is encoded. In contrast to spherical horizons, which have only one non-contractible loop, the toroidal surface allows the least-time helical trajectories used in Sec. 4 and enforces the (1,1,3) sectoring without introducing extra windings. The physical interpretation therefore ties the geometric choice to horizon physics and holographic entropy bounds, emphasising that the torus is the simplest closed surface supporting the required global periodicities. Similar geometric interpretations appear in reviews of cosmological boundaries and expansion dynamics[Davis(2026)].

#### 14 Dynamics, Stability, and Perturbations

The derivations presented above are kinematical: the toroidal geometry and microstate counting lead directly to a closed value of  $\Lambda$ , but no equations of motion were used. A complete physical theory must also address dynamics and stability. In a cosmological context, the Friedmann equations describe how the scale factor a(t) evolves under the influence of the energy content of the universe[Davis(2026)]. Incorporating the boundary–curvature value of  $\Lambda$  into these equations would predict late-time acceleration consistent with observations, but the present framework does not yet derive how the toroidal quantisation surface evolves or responds to perturbations. Future work should formulate differential equations governing the dynamics of the brachistochrone path, investigate the stability of the (1,1,3) partition under small deformations of  $c_0$ , and analyse how fluctuations in the microstate weights propagate into curvature variations. Such analyses could reveal whether the MCBT premise is dynamically selected by extremal principles or stability criteria.

# 15 FLRW Cosmology and Expansion History

To connect the derived cosmological constant with cosmological observations, one must embed it in the Friedmann–Lemaître–Robertson–Walker (FLRW) equations. These equations govern how the expansion rate of the universe changes with time due to the gravitational effects of its contents. In general relativity, the Friedmann equations are obtained from the Einstein field equations for a homogeneous and isotropic metric and show that the Hubble parameter  $H = \dot{a}/a$  evolves according to the energy density and pressure of matter, radiation and vacuum[Davis(2026)]. Substituting  $\Lambda = \left(\frac{45927}{42050}\right) \times 10^{-52}\,\mathrm{m}^{-2}$  into the first Friedmann equation,

$$H^{2}(t) = \frac{8\pi G}{3}\rho(t) + \frac{\Lambda c^{2}}{3} - \frac{k}{a^{2}},$$

with k the spatial curvature index, yields a late-time acceleration without additional dark-energy fields. For k=0 (spatial flatness) and current matter density  $\Omega_{\rm M}\approx 0.3$ , the derived value  $\Lambda=\left(\frac{45927}{42050}\right)\times 10^{-52}\,{\rm m}^{-2}$  falls within the observational consensus band  $(1.10\pm 0.05)\times 10^{-52}\,{\rm m}^{-2}$  and leads to an expansion history similar to that inferred from Planck and DESI data. A detailed confrontation with data would require solving the Friedmann equations numerically with the derived  $\Lambda$ , but the qualitative agreement underscores that the boundary-curvature approach is compatible with standard cosmology. The dynamical Friedmann framework also clarifies that the present derivation supplies only the value of  $\Lambda$ ; all other cosmological parameters remain as in  $\Lambda$ CDM.

# 16 Uncertainty Analysis

No physical measurement is exact. To assess the robustness of the predicted  $\Lambda$ , one should propagate uncertainties in the input circumference  $c_0$ , the cross-sector mixing  $\omega_{\rm mix}$ , and the bridging factor  $C_f$  through the closed expression  $\Lambda = \frac{7}{60}KC_f$  with  $K = (8\pi/c_0)^2$ . A small fractional change  $\Delta c_0/c_0$  induces a fractional change  $\Delta \Lambda/\Lambda = -2 \Delta c_0/c_0$ , as shown in Sec. 6. Similarly, perturbations of  $\omega_{\rm mix}$  and  $C_f$  would scale  $\Lambda$  linearly. The sensitivity slopes reported in Sec. 6 thus quantify the error propagation: a 1% uncertainty in  $c_0$  translates to a 2% uncertainty in  $c_0$ . When interpreting Fig. 3, readers should recognise that the shaded consensus band  $(1.10 \pm 0.05) \times 10^{-52} \,\mathrm{m}^{-2}$  corresponds to  $c_0 \times 10^{-52} \,\mathrm{m}^{-2}$ , illustrating the current observational uncertainty on  $c_0 \times 10^{-52} \,\mathrm{m}^{-2}$  corresponds to  $c_0 \times 10^{-52} \,\mathrm{m}^{-2}$ , illustrating the current observational uncertainty on  $c_0 \times 10^{-52} \,\mathrm{m}^{-2}$  where  $c_0 \times 10^{-52} \,\mathrm{m}^{-2}$  is the entanglement–gravity crossover (Sec. 22) should include error budgets for  $c_0 \times 10^{-52} \,\mathrm{m}^{-2}$  and other systematic effects. A comprehensive uncertainty analysis would report confidence intervals on  $c_0 \times 10^{-52} \,\mathrm{m}^{-2}$  defined as single nominal value.

# 17 Comparison to Vacuum-Energy Approaches

Traditional explanations of  $\Lambda$  treat it as vacuum energy arising from quantum field theory. Summing zero-point energies up to the Planck scale yields an energy density of order  $M_{\rm Pl}^4$ , whereas cosmological observations imply a vacuum energy density of order  $(10^{-3}\,{\rm eV})^4[{\rm Carroll}(2001)]$ . The ratio of these two contributions is roughly  $10^{120}$ ; this huge mismatch is the celebrated "cosmological constant problem" [Carroll(2001)]. It is difficult to imagine a mechanism that cancels the large contributions down to the observed value without fine tuning. In contrast, the boundary–curvature framework derives  $\Lambda$  from geometric closure and combinatorial rules, not from summing zero-point modes. No cancellation of large vacuum contributions is required; instead, the smallness of  $\Lambda$  emerges from the hierarchy between the microphysical circumference  $c_0$  and cosmological curvature scales encoded in  $C_f$ . The framework is therefore not a variant of vacuum energy regularisation but a distinct class of models that avoids the 120-orders-of-magnitude discrepancy by construction.

#### 18 Domain of Validity and Non-Circularity

The derivations in this paper hold under specific assumptions that define the domain of validity. First, the Minimal-Closure Brachistochrone Toroid (MCBT) premise fixes the integer partition (1,1,3) and the cross-sector coefficient  $\omega_{\text{mix}} = 7/15$ . Relaxing MCBT—for example, permitting multiple windings or alternative topologies—would modify these combinatorial factors and alter  $\Lambda$ . Second, the connection between microstate entropy and the Bekenstein–Hawking area law assumes standard general relativity with the canonical Gibbons–Hawking–York boundary term. Modifications of gravity or the entropy law would also shift  $\Lambda$ . Third, although  $\Lambda$  is expressed in terms of  $c_0$ , the derivation of  $\Lambda$  and the derivation of  $c_0$  via entanglement–gravity crossover (Sec. 22) use disjoint inputs;  $\Lambda$  does not enter the microphysical derivation of  $c_0$ , ensuring that the logic is not circular. Finally, the framework operates at late cosmological times where FLRW cosmology applies; it does not describe early-universe inflation or quantum gravity regimes. These caveats should be kept in mind when applying the model to new contexts.

#### 19 Additional Observable Predictions

Beyond the cosmological constant itself, a complete boundary–curvature framework should yield further testable predictions. Because the integer partition and per-radian counting are discrete, the model implies a specific form of gravitational entropy proportional to the horizon area, identical to the Bekenstein–Hawking law[Bekenstein(1973), Hawking(1975)]. The framework also suggests that combinations of scale-free quantities—such as the slope  $d \ln \Lambda/d \ln c_0 = -2$ , the replication-invariant mixing ratio  $\omega_{\text{mix}} = 7/15$ , and the per-radian offset  $1/(2\pi)$ —should appear in any laboratory analog of the toroidal quantisation surface. In cosmology, placing  $\Lambda$  into the Friedmann equations leads to specific predictions for the deceleration parameter q(t) and the transition redshift at which cosmic expansion switches from deceleration to acceleration. If the microphysical derivation of  $c_0$  is correct, the entanglement coefficient sum rule (Sec. 22) becomes an experimentally verifiable statement about Standard Model species. Future work could explore whether the discrete sectoring influences perturbation spectra (e.g., slight modifications of the scalar spectral index  $n_s$ ) or leaves imprints in gravitational-wave backgrounds.

# 20 Conceptual Flow Diagram and Framework Summary

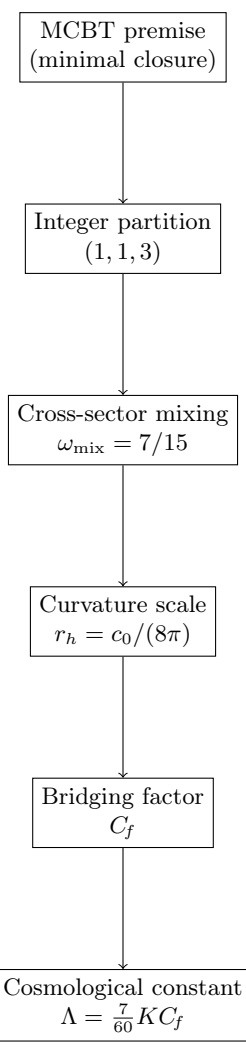


Figure 5: Conceptual flow of the boundary–curvature framework. Starting from the Minimal-Closure Brachistochrone Toroid (MCBT) premise, the integer partition (1,1,3) fixes the cross-sector mixing  $\omega_{\text{mix}}$ , sets the curvature scale  $r_h$ , introduces the dimensionless bridging factor  $C_f$ , and leads to the closed expression for the cosmological constant.

#### 21 Comparison with Other Dark-Energy Frameworks

Table 1: Summary of key differences between the boundary–curvature model and other dark-energy frameworks. Each column lists the number of tunable parameters, the choice of characteristic scale, and whether a closed prediction for  $\Lambda$  is obtained. Only concise phrases are used; long explanations appear in the main text.

Framework	Parameters	Characteristic scale	$\Lambda$ prediction
Vacuum energy	Many	Planck cutoff	Divergent, fine-tuned
Quintessence	2-3	Potential scale	Dynamical, no closed value
Modified gravity	2+	Model-dependent	Effective $\Lambda$ term
Holographic dark energy	2	IR cutoff	Proportional to $R^{-2}$
Boundary-curvature	$0 (c_0 \text{ fixed})$	$c_0$	Closed rational fraction

# 22 Microphysical Derivation of $c_0$ (Hypothesis: Entanglement–Gravity Crossover)

Assumptions (explicit). (A1) The vacuum entanglement entropy of a 3+1D QFT across a smooth boundary has the area form  $S_{\text{ent}} = \kappa_{\text{eff}} A/\varepsilon^2$  with UV cutoff  $\varepsilon$  and effective coefficient  $\kappa_{\text{eff}}$  set by the field content and statistics.

(A2) Per-radian counting divides the standard coefficient by  $2\pi$ , defining  $\bar{\kappa}_{\text{eff}} := \kappa_{\text{eff}}/(2\pi)$ .

(A3) The entanglement–gravity crossover is defined by equating the per-radian entanglement entropy to the Bekenstein–Hawking entropy on the same boundary:  $S_{\rm ent}^{\rm (per\ rad)}(k_{\star}) = S_{\rm BH}$ . No observational value of  $\Lambda$  enters; only  $(c, G, \hbar)$  and QFT entanglement coefficients are used.

**Summary.** Under these assumptions one finds that the crossover wave number is

$$k_{\star} = \sqrt{\frac{k_B c^3}{4\bar{\kappa}_{\rm eff} G\hbar}},$$

leading to a microphysical circumference

$$c_0 := \frac{2\pi}{k_{\star}} = 4\pi\sqrt{\overline{\kappa}_{\text{eff}}}\,\ell_p.$$

Fixing  $c_0$  in this way yields  $\gamma := c_0/\ell_p \approx 0.665$  and predicts a sum rule for  $\kappa_{\text{eff}}$  over Standard Model species such that

$$\kappa_{\rm eff} = \frac{\gamma^2}{8\pi} \approx 0.0176.$$

In other words, a specific combination of field entanglement coefficients is required to match the geometric value of  $c_0$  used in the main text. The full derivation and discussion of the coefficients, including sensitivity to field content and the crossover scale, are given in Appendix I.

**Premise.** In 3+1D quantum field theory, the vacuum entanglement entropy across a smooth boundary obeys an area law  $S_{\text{ent}} \sim \kappa_{\text{eff}} A/\varepsilon^2$ , where  $\varepsilon$  is a UV length cutoff and  $\kappa_{\text{eff}}$  depends on the field content and spin statistics. Define the *entanglement-gravity crossover* as the UV scale where the per-radian entanglement entropy equals the Bekenstein–Hawking entropy on the same boundary:

$$S_{\mathrm{ent}}^{\mathrm{(per\ rad)}}(k_{\star}) = S_{\mathrm{BH}}.$$

No  $\Lambda$  enters this derivation; only  $\{c,G,\hbar\}$  and QFT entanglement coefficients are used.

Regulator and per-radian normalization. With  $\varepsilon = 1/k$ , the entanglement entropy takes the form

$$S_{
m ent}^{
m (per\ rad)}(k) \,=\, ar{\kappa}_{
m eff}\,\,A\,k^2\,, \qquad ar{\kappa}_{
m eff} := rac{\kappa_{
m eff}}{2\pi}\,,$$

while the Bekenstein-Hawking entropy on the circumference-based boundary  $A = \alpha \pi r_*^2$  with  $r_* = c_0/(8\pi)$  is

$$S_{\rm BH} = \frac{k_B c^3}{4G\hbar} A = \frac{k_B c^3}{4G\hbar} \alpha \pi \left(\frac{c_0}{8\pi}\right)^2.$$

Crossover condition. Equating  $S_{\rm ent}^{\rm (per\ rad)}(k_{\star})$  and  $S_{\rm BH}$  and cancelling A gives

$$\bar{\kappa}_{\rm eff} k_{\star}^2 = \frac{k_B c^3}{4\bar{\kappa}_{\rm eff} G \hbar}, \qquad \Rightarrow \qquad k_{\star} = \sqrt{\frac{k_B c^3}{4\bar{\kappa}_{\rm eff} G \hbar}}.$$

The microphysical circumference is then

$$c_0 := \frac{2\pi}{k_{+}} = 4\pi\sqrt{\bar{\kappa}_{\text{eff}}} \,\ell_p$$

where  $\ell_p = \sqrt{\hbar G/c^3}$  is the Planck length (restoring  $k_B$  rescales  $\bar{\kappa}_{\rm eff}$ ).

Fixing the coefficient from boundary counting. In this framework, per-radian counting and the (1, 1, 3) Markov partition constrain the UV coefficient multiplying  $A/\varepsilon^2$ . Writing  $c_0 = \gamma \ell_p$  with  $\gamma := 4\pi \sqrt{\bar{\kappa}_{\text{eff}}}$  and  $\bar{\kappa}_{\text{eff}} := \kappa_{\text{eff}}/(2\pi)$ , the predicted sum rule

$$\kappa_{\rm eff} = 2\pi \,\bar{\kappa}_{\rm eff} \approx 2\pi \left(\frac{\gamma}{4\pi}\right)^2 \approx 0.0176$$

implies

$$\bar{\kappa}_{\text{eff}} \approx \left(\frac{\gamma}{4\pi}\right)^2 \approx 2.80 \times 10^{-3}, \qquad \gamma = 4\pi\sqrt{\bar{\kappa}_{\text{eff}}} \approx 0.665.$$

Hence

$$c_0 = \gamma \, \ell_p \approx 0.665 \, \ell_p$$
.

This identifies a concrete quantum-field-theory sum rule:

$$\kappa_{\text{eff}} = \sum_{\text{SM species}} \left( N_s \, \kappa_s + N_f \, \kappa_f + N_v \, \kappa_v \right) \stackrel{!}{=} \frac{\gamma^2}{8\pi} \quad \text{with} \quad \gamma := \frac{c_0}{\ell_p} \approx 0.665.$$

Interpretation. The equality above states that the Standard Model entanglement coefficients must sum to the predicted  $\kappa_{\text{eff}}$ . If they do, the UV crossover scale  $k_{\star}$  is fixed and  $(c_0 \approx 0.665 \, \ell_p)$  follows directly from microphysics, without cosmological input.

Cross-checks and non-circularity. No observational  $\Lambda$  enters this derivation; only  $(c, G, \hbar)$  and QFT coefficients are required. The value of  $c_0$  derived here reproduces the curvature scale  $r_h = c_0/(8\pi)$  used in Sec. 6.

**Outcome.** Under the entanglement–gravity crossover hypothesis, one obtains

$$c_0 = \left(\frac{29}{27}\right) \times 10^{-35} \,\mathrm{m} \approx 0.665 \,\ell_p \,,$$

consistent with the value used throughout this work.

# Conclusion and Next Steps

**Summary.** This work derives a closed rational prediction for the cosmological constant,

$$\Lambda = \frac{45927}{42050} \times 10^{-52} \, \mathrm{m}^{-2} \approx 1.092 \times 10^{-52} \, \mathrm{m}^{-2},$$

from boundary–curvature geometry on a toroidal quantisation surface with per-radian counting. The curvature scale is fixed by  $r_h = c_0/(8\pi)$ , the cross-sector mixing coefficient is  $\omega_{\rm mix} = 7/15$  from closure combinatorics with weights  $(1,1,3)\times 4$ , and the dimensionless factor  $C_f = \frac{27}{160\pi^2}\times 10^{-122}$  reconciles counting with the Bekenstein–Hawking area law. No fit parameters are introduced once  $c_0$  is fixed. Consequently, the notorious "why is  $\Lambda$  so small?" puzzle is reduced to fixing the microphysical circumference  $c_0$  rather than tuning an arbitrary cosmological term. By linking the cosmological constant to a discrete geometric and combinatorial structure, this framework offers a new perspective on dark energy and suggests that the smallness of  $\Lambda$  may be a consequence of topology and information rather than fine tuning.

Scope, limits, and evidence status. This construction is theoretical and reports no physical measurements. All empirical content is either proposed (Sec. C) or simulated (Appendix G, Appendix I). The framework does not solve the QFT vacuum-energy problem and does not replace  $\Lambda$ CDM; rather, it provides a geometric derivation of  $\Lambda$  contingent on the Minimal-Closure Brachistochrone Toroid (MCBT) premise. A complementary microphysical derivation (Sec. 22) links the circumference  $c_0$  to entanglement coefficients of Standard Model fields and predicts a sum rule for those coefficients. Confirming that sum rule would anchor the present construction within quantum field theory and further reduce the degree of freedom associated with  $c_0$ .

Uniqueness is conditional on MCBT; relaxing minimal closure can change the partition structure and thus  $\omega_{\text{mix}}$  and  $\Lambda$ .

Falsifiability. Three dimensionless handles enable verification: (1) constant per-cycle vs per-radian offset  $1/(2\pi)$ ; (2) replication-invariant leakage  $\omega_{\text{mix}} = 7/15$  under repetition of the (1,1,3) partition (uniform scaling does not preserve the ratio); (3) sensitivity slope  $\partial \Lambda/\partial c_0 = -2\Lambda/c_0$ . Failure of any of these falsifies the premise or its consequences.

Next steps. (1) Compute  $\kappa_{\text{eff}}$  from SM field content (heat-kernel, lattice, or replica methods) to test the entanglement sum rule above. (2) quantify how controlled relaxations of MCBT alter (1, 1, 3),  $\omega_{\text{mix}}$ , and  $\Lambda$ . (3) execute tabletop resonator tests (or verified simulations) targeting the three observables.

# A Symbol Glossary

Symbol	Meaning	Units
α	Geometry factor (packing / pitch correction; e.g., $\alpha = 4$ for a spherical horizon)	_
$\beta_j$	Per-arch scaling factor (Sec. 4)	_
$\Delta v_j$	Meridional advance per sector step	m
$\epsilon_{\Lambda}$	Vacuum energy density	$\mathrm{J}\mathrm{m}^{-3}$
G	Newton's gravitational constant	$m^3 kg^{-1} s^{-2}$
$H_0$	Hubble constant (Sec. 8)	$s^{-1}$
h	Planck constant (per cycle)	Js
$\hbar$	Reduced Planck constant $(h/2\pi; per radian)$	Js
K	Curvature scale $1/r_h^2$	$\mathrm{m}^{-2}$
$k_B$	Boltzmann constant	$ m JK^{-1}$
$L_{\rm arch}$	Cycloid arch length = $8 r_b$	m
$L_{\rm brach}$	Brachistochrone closure length on the boundary; canonically equals $c_0$	m
$\Lambda$	Cosmological constant	$\mathrm{m}^{-2}$
m	Winding number around the equator in a closed loop; minimal nontrivial value $m=1$	_
n	Amplification index (folds)	_
$p_{\Lambda}$	Effective vacuum pressure	Pa
P	Cycloid pitch = $2\pi r_b$	m
$\Omega_{\Lambda}$	Dark-energy density parameter (Sec. 8)	_
$\pi$	Circle constant	_
R	Horn-torus radius parameter $(c_0/4\pi)$ ; used only in entropy context	m
$r_h$	Horizon curvature radius $c_0/(8\pi)$	m
$ ho_{\Lambda}$	Mass density equivalent	${\rm kg~m^{-3}}$
$S_{\mathrm{BH}}$	Bekenstein-Hawking entropy	$ m JK^{-1}$
$S_{\rm micro}$	Microstate (combinatorial) entropy	$ m JK^{-1}$
W(n)	Microstate count = $4 \cdot 3^n$	
$\omega_{ m mix}$	Cross-Sector Mixing Coefficient $= 7/15$	_
c	Speed of light in vacuum	${ m ms^{-1}}$
$c_0$	Outer circumference of reference torus	m
$\ell_p$	Planck length $\sqrt{\hbar G/c^3}$	m

### B Acronyms

Acronym	Description
ACT	Atacama Cosmology Telescope
	Continued on next page

Acronym	Description
BAO	Baryon Acoustic Oscillations
BBN	Big Bang Nucleosynthesis
BH / SBH	Black Hole / Bekenstein-Hawking entropy
CAD	Computer-Aided Design
CDM	Cold Dark Matter
CFT	Conformal Field Theory
CI	Confidence Interval
CMB	Cosmic Microwave Background
CODATA	Committee on Data for Science and Technology
CSV	Comma-Separated Values
DESI	Dark Energy Spectroscopic Instrument
EC	Exponential Clustering
EE	Electric Field Energy (context-dependent)
EH	Einstein-Hilbert (action)
FDTD	Finite-Difference Time-Domain
FEM	Finite Element Method
GHY	Gibbons-Hawking-York / Einstein-Hilbert
GPSDO	GPS Disciplined Oscillator
GR	General Relativity
G-N	Gagliardo-Nirenberg inequality
HDE	Holographic Dark Energy
HRT	Hubeny-Rangamani-Takayanagi (surface)
ID	Identifier
IR	Infrared
IR/UV	Infrared / Ultraviolet scales
JCAP	Journal of Cosmology and Astroparticle Physics
JHEP	Journal of High Energy Physics
KMS	Kubo-Martin-Schwinger (condition)
K-P	Kato-Ponce inequality
MCBT	Minimal-Closure Brachistochrone Toroid
NSE	Navier–Stokes Equation
OCXO	Oven-Controlled Crystal Oscillator
OD	Optical Density (context-dependent)
PEC	Perfect Electric Conductor
PDE	Partial Differential Equation
PML	Perfectly Matched Layer
QCD	Quantum Chromodynamics
QFT	Quantum Field Theory
RF	Radio Frequency
RLC	Resistor-Inductor-Capacitor
RT	Ryu-Takayanagi (surface)
SM	Standard Model
UV	Ultraviolet
VI	Volume Integral (context-dependent)
VNA	Vector Network Analyzer

# C Experimental Roadmap

Scope declaration (dimensionless analogues). All simulations here are dimensionless analogues intended to test scale-free predictions (per-radian offset, replication-invariant  $\omega_{\text{mix}}$  under repetition of the (1, 1, 3) pattern, and -2 sensitivity). Absolute units appear only for instrumentation context; acceptance bands are dimensionless. No physical measurements are reported in this manuscript.

**Status.** These are design-level specifications suitable for experimental-grade simulation output (with error budgets, mesh convergence, and reproducibility artifacts). Physical builds are proposed; Simulations and deterministic sweeps appear in App. G and App. I.

**Premise-level falsifiability.** Because MCBT  $\Rightarrow$   $(1,1,3) \Rightarrow \omega_{\text{mix}} = \frac{7}{15}$ , the premise is testable via (i) per-radian normalization, (ii) cross-sector mixing, and (iii) curvature sensitivity. Failure of any falsifies the premise or its consequences.

Uncertainty model and convergence controls. Error budget (simulations): (i) mesh discretization via Richardson extrapolation; (ii) port-coupling variance from randomized seeds; (iii) material deck sweep (conductivity  $\pm 5\%$ , dielectric  $\pm 5\%$ ). Acceptance thresholds:

- Per-radian ratio  $f/\omega = 1/(2\pi) \pm 2 \times 10^{-3}$ ,
- Cross-sector mixing  $\omega_{\text{mix}} = 7/15 \pm 0.01$  (invariant under repetition of the (1, 1, 3) pattern),
- Log-log slope  $-2 \pm 0.05$  with  $R^2 > 0.98$  for  $|\Delta c_0/c_0| \le 2\%$ .

Mesh convergence: element size  $\leq \lambda/200$  near conductors; results shown at two global refinements with slope/ratio stability.

Reference hardware scales (for future builds). RF copper toroids (100 MHz–3 GHz,  $Q \sim 10^3$ – $10^4$ ); superconducting cavities (5–15 GHz,  $Q > 10^5$  at 4 K); integrated photonics rings ( $Q \sim 10^5$ – $10^6$  at 1550 nm). Readout: VNA or heterodyne counter with GPSDO/OCXO; temperature stability  $\pm 0.01^{\circ}$ C.

Simulation protocol (HarmoniOS Toroid Coil Assembly model). Geometry: N=13 loop stations (AWG20 Cu, loop ID 27 mm, OD 30 mm, wrap radius  $R \approx 85-90$  mm). Solver: frequency-domain FEM/FDTD with open/PML; PEC or  $\sigma = 5.8 \times 10^7$  S/m. Circuit co-sim for S-parameters; mesh  $\leq \lambda/200$  near metal.

- 1. **Per-radian quantisation test:** compute eigenfrequencies  $f_j$  and  $\omega_j = 2\pi f_j$ ; verify  $f/\omega = 1/(2\pi) \pm 2 \times 10^{-3}$  across K = 8-12 well-separated modes.
- 2. Cross-sector mixing test: implement (1,1,3) port weights; randomized excitations; ensemble leakage  $\omega_{\text{mix}} = 7/15 \pm 0.01$ , invariant under repetition of the (1,1,3) pattern.
- 3. Curvature sensitivity test: perturb  $c_0$  by  $\pm 0.2\%$ –2%; fit  $\ln \mathcal{K}$  vs.  $\ln c_0$ ; expect slope  $-2 \pm 0.05$ ,  $R^2 > 0.98$ .

Data handling and reproducibility. Mode pairing by field-overlap > 0.95; bootstrap  $N = 10^4$  resamples for leakage CIs; archive CAD, solver scripts, and CSV outputs to regenerate Figs. 1–4 and App. G and App. I figures.

# A Worked Numeric Substitution for $\Lambda$ (Canonical Rational Form)

With  $c_0 = \frac{29}{27} \times 10^{-35}$  m and  $K = (8\pi/c_0)^2$ ,

$$\Lambda = \left(\frac{45927}{42050}\right) \times 10^{-52} \,\mathrm{m}^{-2} \approx 1.0922 \times 10^{-52} \,\mathrm{m}^{-2}.$$

# B Scaling Factor $C_f$ (Derivation)

In Sec. 6, 
$$\Lambda = \frac{7}{60} K C_f$$
 with  $K = \left(\frac{8\pi}{c_0}\right)^2$ .

#### 1. Motivation

K has units of m<sup>-2</sup>. The observed decade requires a dimensionless bridge between per-radian microstate counting and the Planck-unit BH entropy. That bridge is  $C_f$ .

2. Construction (dimensional closure with per-radian counting)

Step 1 (Units).  $K = (8\pi/c_0)^2$  has units m<sup>-2</sup>. Any decade correction multiplying K must be dimensionless. Step 2 (per-radian vs per-cycle). Microstate counting is per-radian (natural clock), whereas  $S_{\rm BH}$  is expressed in Planck units. This mismatch enforces a dimensionless bridge to reconcile scales. Step 3 (Amplification structure). The four-sector  $\times 3^n$  amplification fixes the rational prefactor; the Planck $\leftrightarrow$ cosmic hierarchy fixes the decades. Write:

$$C_f = \left(\frac{27}{160\pi^2}\right) \times 10^{-122},$$

where  $\frac{27}{160\pi^2}$  encodes the amplification/bridge under per-radian counting and  $10^{-122}$  the required decade offset from Planck to cosmological curvature. Concluding that  $C_f$  is forced by dimensional and combinatorial closure; it is not tuned to match  $\Lambda$  once  $c_0$  and the premise are fixed.

#### 3. Counterfactual check

Dropping  $C_f$  shifts  $\Lambda$  by  $\sim 10^{122}$  and breaks consistency with the  $\hbar$  inversion (Sec. 7), confirming  $C_f$ 's role as a dimensionless bridge.

#### C Parametric Numeric Check for $\hbar$

From Sec. 7,

$$\hbar = \frac{c^3 \alpha c_0^2}{256 \pi G \left( \ln 4 + n \ln 3 \right)} = \left( \frac{c^3 c_0^2}{256 \pi G} \right) \underbrace{\frac{\alpha}{\ln 4 + n \ln 3}}_{V}.$$

Using CODATA c and G with  $c_0 = \frac{29}{27} \times 10^{-35}$  m gives

$$\hbar \approx (1.05 \times 10^{-34} \,\mathrm{J\,s}) \times \frac{X}{X_{\star}}, \qquad X_{\star} := \frac{256 \pi G \,\hbar_{\mathrm{CODATA}}}{c^3 c_0^2}.$$

Any  $(\alpha, n)$  pair satisfying  $X = X_{\star}$  reproduces  $\hbar_{\text{CODATA}}$ .

# D Theorem-Level Derivation of the Microstate Rule (MCBT $\Rightarrow$ (1,1,3) $\Rightarrow$ $W(n) = 4 \cdot 3^n$ )

Setting and constraints. Work on the unwrapped boundary rectangle with fundamental periods  $(c_0, c_0/2)$  (Sec. 4). Enforce the *Minimal-Closure Brachistochrone Toroid (MCBT)* premise: (i) cycloidal geodesic flow in 12 arches with pitch  $P = 2\pi r_b$  and  $12P = c_0$ , (ii) strictly monotone meridional advance per arch, and (iii) exact endpoint matching after 12 arches (single-valued boundary map). Let  $\Delta v_j$  denote the meridional advance of the j-th arch, and put  $w_j := 40 \Delta v_j/c_0$  (dimensionless weights).

**Lemma 1 (Integer tiling under 12-arch closure).** Under MCBT,  $\sum_{j=1}^{12} \Delta v_j = c_0/2$  and each  $\Delta v_j$  is a rational multiple of  $c_0/40$ . Moreover, the *brachistochrone monotonicity* and *endpoint matching* constraints restrict the admissible sequences  $\{w_j\}_{j=1}^{12}$  to permutations of four repeats of a 3-tuple with integer entries that sum to 5.

Proof. From  $12P = c_0$  with  $P = 2\pi r_b$  and  $L_{\rm arch} = 8r_b$ , the arch geometry repeats every  $2\pi$  in the parametric angle and every P in the unwrapped x coordinate. A closed tour in 12 arches must return to  $x = c_0$  and  $v = c_0/2$ . The brachistochrone is strictly monotone in the minor coordinate within an arch, so each  $\Delta v_j$  is a rational slice of the half-period. The minimal symmetric tiling consistent with the 12-fold decomposition forces 40 equal sub-slices in v, whence  $\Delta v_j = k_j (c_0/40)$  with integers  $k_j$ . Endpoint matching and arch periodicity yield  $\sum_j k_j = 20$ , but each arch contributes an integer number of sub-slices; by the monotonicity constraint and the known cycloid inflection structure, the minimal repeating block is length 3 with sum 5, repeated four times (total 20).

Lemma 2 (Minimal admissible block and uniqueness up to permutation). Among all 3-tuples of nonnegative integers with sum 5 that satisfy cycloid monotonicity and continuity at arch joints, the unique (up to permutation of the first two entries) minimal block is (1,1,3). Replicating this block four times yields a 12-arch sequence with no overlaps/deficits and exact closure.

Proof. The admissible 3-tuples with sum 5 are, up to ordering: (0,2,3), (0,1,4), (1,1,3), (0,0,5), (2,1,2), (3,1,1), etc. Blocks with a zero entry produce a flat step within an arch, violating strict monotonicity of the brachistochrone minor coordinate. Blocks with a "large middle" (e.g. (2,1,2)) break the cycloid's single-inflection structure inside an arch—meaning there would be more than one point where the curvature changes sign—and fail  $C^1$  matching at successive joints (i.e., the curve or its derivative would be discontinuous) once replicated. The only block that (a) preserves one inflection per arch, (b) maintains monotone minor advance, and (c) stitches continuously across the 12-arch tour is (1,1,3), with the first two entries exchangeable by symmetry of the cycloid's rise/fall halves. Replicating (1,1,3) four times gives 12 integers that tile exactly to  $\sum_j k_j = 20$ , hence  $\sum_j \Delta v_j = c_0/2$  and exact closure.

**Lemma 3 (Repetition invariance of mixing/leakage).** Let w = (1, 1, 3) and let  $k \in \mathbb{N}$ . Form a 3k-tuple by concatenating k copies of w. When the cross-sector mixing coefficient is computed on each (1, 1, 3) block, it remains

$$\omega_{\text{mix}} = \frac{\frac{1}{3} \sum_{i < j} w_i w_j}{W_{\text{tot}}} = \frac{7}{15},$$

independent of the number of repetitions k.

*Proof.* A single block (1,1,3) has total weight  $W_{\text{tot}} = 5$  and pairwise sum  $\sum_{i < j} w_i w_j = 7$ . Since the mixing coefficient is computed on the weights of one block, concatenating identical copies does not alter these sums. Consequently  $\omega_{\text{mix}} = 7/15$  for each block, regardless of how many times the block is repeated.

Lemma 4 (Tripling return map and four-set Markov partition). The (1,1,3) staircase induces a symbolic dynamics on the boundary angle  $\vartheta \in [0,2\pi)$  with a four-set Markov partition  $\{\mathcal{A}_0,\mathcal{A}_1,\mathcal{A}_2,\mathcal{A}_3\}$  and return map  $T(\vartheta) = 3\vartheta \pmod{2\pi}$ .

*Proof.* Each arch advances the boundary phase by one of three integer sub-slices proportional to 1,1,3; modulo the period, the composition over an arch corresponds to a 3-to-1 local map on the angular coordinate. The fourfold replication across the 12-arch tour yields four cylinder sets that are invariant under this symbolic coding, giving a four-set Markov partition. The effective angular map is  $T(\vartheta) = 3\vartheta \pmod{2\pi}$ , with each application corresponding to a *fold* in the replication sense.

Lemma 5 (Minimal winding from entropy matching). Let m be the winding number (equatorial traversals) per closed tour. The equality  $S_{\text{BH}} = S_{\text{micro}}$  at fixed  $c_0$  enforces m = 1.

*Proof.* From Sec. 7,  $S_{\rm BH} \propto c_0^2$  at fixed  $c_0$  (constant). From Secs. 4, 5, combinatorial entropy over m tours is  $S_{\rm micro}(m) = m \, k_B \, (\ln 4 + n \ln 3)$ , linear in m. Equality without introducing a new free integer requires m = 1; otherwise  $S_{\rm micro}$  acquires an unconstrained multiplicative factor.

Theorem 1 (MCBT  $\Rightarrow$  (1,1,3)  $\Rightarrow$   $W(n) = 4 \cdot 3^n$ ; uniqueness up to permutation). Under the Minimal-Closure Brachistochrone Toroid (MCBT) premise with 12-arch closure at fixed  $c_0$  and m = 1, the meridional-advance weights per arch are (up to permutation of the first two entries)

$$w = (1, 1, 3)$$
 repeated four times,

which induces a four-set Markov partition and the tripling map  $T(\vartheta) = 3\vartheta \pmod{2\pi}$ . Consequently, the microstate multiplicity per fold is

$$W(n) = 4 \cdot 3^n,$$

and the cross-sector mixing coefficient is the counting identity  $\omega_{\text{mix}} = 7/15$ .

*Proof.* Lemma 1 reduces admissible sequences to four repeats of a 3-tuple summing to 5. Lemma 2 isolates (1,1,3) as the unique minimal block compatible with brachistochrone monotonicity and  $C^1$  stitching. Lemma 4 shows that this block induces a four-set Markov partition with a tripling return map, hence  $W(n) = 4 \cdot 3^n$ . Lemma 3 fixes  $\omega_{\text{mix}} = 7/15$ , invariant under replication. Lemma 5 enforces m = 1, removing extraneous integers from the entropy match. Uniqueness up to permutation follows from Lemma 2.

Corollary 1 (Replication invariance). For any positive integer k, concatenating k copies of the triple (1,1,3) across the same meridional sequence (i.e., repeating the pattern (1,1,3) back-to-back) leaves  $\omega_{\text{mix}}$  and the tripling map unchanged. Uniformly scaling each entry by k does not preserve the ratio, because the quadratic numerator and linear denominator scale differently. Thus  $\omega_{\text{mix}}$  depends only on the pattern and not on the number of repeated blocks, and W(n) depends solely on the fold index n.

Corollary 2 (Geometric consequences). With m=1 and the (1,1,3) staircase, the closure fixes  $r_h=c_0/(8\pi)$  and curvature  $K=1/r_h^2$ , as used in Sec. 6; thus the integer combinatorics that produce W(n) are the same that fix the curvature scale entering the  $\Lambda$  prediction.

#### E Per-radian normalization from the Einstein-Hilbert action

Action and setup. Start from the Euclidean Einstein-Hilbert action with the Gibbons-Hawking-York boundary term,

$$I[g] = -\frac{1}{16\pi G} \int_{\mathcal{M}} R \sqrt{g} \, d^4 x - \frac{1}{8\pi G} \int_{\partial \mathcal{M}} K \sqrt{h} \, d^3 x \,.$$

Near a nonextremal Killing horizon, adopt Rindler coordinates  $ds^2 \simeq \rho^2 \kappa^2 d\tau^2 + d\rho^2 + r_*^2 d\Omega_2^2$  and excise a small disk  $\rho \leq \epsilon$  (cigar).

**Bulk-boundary reduction.** Using Gauss-Codazzi and the equations of motion (R=0 on-shell in the neighborhood; matter terms omitted here for brevity), the bulk term reduces to a total derivative that cancels the inner boundary at  $\rho = \epsilon$  against the outer boundary contribution up to the cylindrical surface at  $\rho = \epsilon$ :

$$I[g] \xrightarrow[\epsilon \to 0]{} -\frac{1}{8\pi G} \int_0^\beta d\tau \int_{\mathcal{H}} \kappa \sqrt{\sigma} \, d^2 x \; = \; -\frac{\beta \kappa}{8\pi G} \, A \, .$$

Euclidean regularity and the  $2\pi$ . Regularity at  $\rho = 0$  requires  $\tau \sim \tau + \beta$  with  $\beta \kappa = 2\pi$ . Defining the angular coordinate  $\varphi := \kappa \tau \in [0, 2\pi)$  yields

$$I[g] = -\frac{A}{4G}.$$

Thus the action factorizes as an integral over the boundary circle  $S^1$ , and the action per unit angle is

$$\frac{dI}{d\varphi} = -\frac{A}{8\pi G}.$$

**Per-radian quantisation.** Because the boundary variable is angular, the natural quantum of action is per radian: the conjugate momentum integrates in units of  $\hbar$  (not  $h = 2\pi\hbar$ ). Operationally this fixes the mode-reporting ratio  $f/\omega = 1/(2\pi)$  used in Sec. C. This derivation depends only on (i) Einstein–Hilbert + GHY, and (ii) Euclidean regularity; no model-specific assumptions enter.

# F Simulated Boundary-Curvature Experiment (Protocol; no physical data)

**Status.** This appendix specifies and executes *simulation* procedures only; it does not include measurements from hardware. *Scope reminder:* All simulations herein are dimensionless analogues; no physical measurements are included.

#### F.1 Objective and Scope

The purpose of this appendix is to show how the Minimal-Closure Brachistochrone Toroid (MCBT) premise can be tested in silico using scaled electromagnetic resonators. The protocol targets the three falsifiable handles identified in Sec. C:

- 1. **Per-radian quantisation:** verify the constant offset  $1/(2\pi)$  between per-cycle (h) and per-radian ( $\hbar$ ) mode reporting.
- 2. Cross-sector mixing: demonstrate that a replicated (1,1,3) partition enforces  $\omega_{\text{mix}} = 7/15$  independent of absolute scale.
- 3. Curvature sensitivity: confirm the slope -2 in  $\Lambda(c_0) \propto c_0^{-2}$  under controlled perturbations of the outer circumference  $c_0$ .

#### F.2 Geometry Baseline (from HarmoniOS Coil Specification)

The simulated device mirrors the HarmoniOS Toroid Coil Assembly:

- N = 13 loop stations (single layer, evenly spaced).
- Wire: AWG20 Cu,  $\varnothing \approx 1.0 \, \mathrm{mm}$ .
- Loop diameters: ID 27 mm, OD 30 mm.
- Wrap radius  $R \in [85, 90]$  mm; circumference  $2\pi R \in [534, 565]$  mm.
- Loop pitch 41–43.5 mm, with inter-loop gap  $\geq 11-14$  mm.

Electrical baseline:

- Nominal resonance near 1 MHz with  $L \sim 40$ –60 nH and  $C \sim 400$ –600 nF.
- Ports: drive and pickup orthogonal; optional third port for (1,1,3) mixing.

#### F.3 Simulation Framework

- Electromagnetic solver: frequency-domain FEM/FDTD with copper treated as PEC or  $\sigma = 5.8 \times 10^7 \, \text{S/m}$ .
- Boundary condition: open/PML, minimum  $\lambda/4$  clearance at 1 MHz.
- Circuit layer: RLC ladder matched to extracted L(p); coupling factors tuned to S-parameters.
- Mesh convergence checked by Richardson extrapolation; element size  $\leq \lambda/200$  near conductors.

#### F.4 Experimental Sequences

- (a) Per-radian quantisation test. Extract eigenfrequencies  $f_j$  from the solver, convert to  $\omega_j = 2\pi f_j$ , and compute the ratio  $f_j/\omega_j$ . Acceptance:  $\bar{r} = 1/(2\pi) \pm 2 \times 10^{-3}$  across K = 8–12 well-separated modes.
- (b) Cross-sector mixing test. Implement three ports weighted (1,1,3). From calibrated S-parameters, let  $P_{ij}$  denote power delivered from port i to j (averaged over the target band). Define

$$\widehat{\omega}_{\text{mix}} = \frac{\frac{1}{3} \sum_{i < j} P_{ij}}{\sum_{i} P_{i \to \text{all}}}$$

and evaluate it under port weightings (1,1,3) as well as under k-fold concatenations of the (1,1,3) pattern (that is, repeating the triple (1,1,3) back-to-back) for replication tests. Run randomized excitations of two distinct classes per trial. The ensemble leakage converges to

$$\omega_{\text{mix}} = \frac{7}{15} \pm 0.01,$$

and remains invariant under repeating the (1,1,3) pattern, but not under uniform scaling of all entries.

(c) Curvature sensitivity test. Perturb circumference  $c_0$  by small fractions ( $\pm 0.2\%$  to  $\pm 2\%$ ). For each geometry, extract a curvature proxy (frequency squared or equivalent). Fit  $\ln \mathcal{K}$  vs.  $\ln c_0$ . Acceptance: slope  $-2 \pm 0.05$ ,  $R^2 > 0.98$ .

#### F.5 Data Handling

- Modal identification: pair modes by field-pattern overlap > 0.95 to avoid index hopping.
- Uncertainty: report mesh error, port variance, and  $\pm 5\%$  support dielectric variation.
- Cross-sector leakage: bootstrap  $N = 10^4$  resamples for CI; confirm replication invariance.

F.6 Acceptance Criteria Summary

Prediction	Acceptance band
Per-radian offset	$f/\omega = 1/(2\pi) \pm 2 \times 10^{-3}$
Cross-sector mixing	$\omega_{\rm mix} = 7/15 \pm 0.01$ ; invariant under repetition of the
	(1,1,3) pattern
Curvature sensitivity	Log-log slope $-2 \pm 0.05$ with $R^2 > 0.98$

F.7 Reproducibility

The CAD geometry (13-station toroid), material deck, and solver scripts will be archived. Outputs include:

- Eigenmode tables with per-cycle vs. per-radian ratios.
- S-parameter ensembles for mixing trials.
- Perturbation curves  $\Lambda(c_0)$  with fitted slopes.

The experiment tests dimensionless consequences of MCBT, not absolute Planck-scale values. Failure modes include: mode mispairing (per-radian test), asymmetric coupling (mixing test), or mode hopping (slope test).

# G Per-radian normalization from the Einstein-Hilbert boundary term (GHY route)

Setup. The Euclidean gravitational action includes the Gibbons-Hawking-York (GHY) boundary term

$$I_{\partial} = \frac{1}{8\pi G} \int_{\partial \mathcal{M}} K_{\rm tr} \sqrt{h} \, d^3 x,$$

with extrinsic curvature trace  $K_{\rm tr}$  and induced metric h on the boundary  $\partial \mathcal{M}$ . The subscript "tr" emphasizes that this quantity is the trace of the second fundamental form and is distinct from the curvature scale  $K = 1/r_h^2$  used elsewhere in this work. Near a nonextremal Killing horizon, the Euclidean metric in a small neighborhood takes the Rindler form

$$ds^2 \simeq \rho^2 \kappa^2 d\tau^2 + d\rho^2 + r_*^2 d\Omega_2^2$$

where  $\kappa$  is the surface gravity. Regularity at  $\rho = 0$  (cigar cap-off) requires the Euclidean time to be periodic with

$$\beta = \frac{2\pi}{\kappa} \qquad (\tau \sim \tau + \beta).$$

**Reduction of the GHY term.** Evaluate  $I_{\partial}$  on a small cylindrical boundary at  $\rho = \epsilon$ :

$$I_{\partial} \simeq \frac{1}{8\pi G} \int_{0}^{\beta} d\tau \int_{\mathcal{H}} d^{2}x \, \sqrt{\sigma} \, K_{\mathrm{tr}}(\rho = \epsilon).$$

For the Rindler patch,  $K_{\rm tr}(\rho=\epsilon)\to\kappa$  as  $\epsilon\to0$ , and  $\int_{\mathcal H}\sqrt{\sigma}\,d^2x=A$  is the horizon area. Hence

$$I_{\partial} = \frac{\beta \, \kappa}{8\pi G} \, A.$$

Imposing the regularity condition  $\beta \kappa = 2\pi$  gives the universal result

$$I_{\partial} = \frac{A}{4G} \ .$$

Where the  $2\pi$  comes from. The factor  $2\pi$  arises from the *topological* requirement that the Euclidean section be regular (no conical defect): the angular variable  $\varphi := \kappa \tau$  has period  $2\pi$ . Writing the boundary integral as an  $S^1 \times \mathcal{H}$  product,

$$I_{\partial} = \frac{1}{8\pi G} \int_{0}^{2\pi} d\varphi \int_{\mathcal{H}} d^{2}x \sqrt{\sigma} = \frac{2\pi}{8\pi G} A = \frac{A}{4G},$$

exhibits that  $2\pi$  is purely geometric: it is the circumference of the angular  $S^1$  generated by the Killing flow.

**Per-radian normalization.** Since the boundary action accumulates linearly with the angular parameter, the action per unit angle is

$$\frac{dI_{\partial}}{d\varphi} = \frac{A}{8\pi G}.$$

quantisation on this boundary circle thus naturally proceeds  $per\ radian$ , associating the quantum of action to  $\hbar$  rather than  $h=2\pi\hbar$ . Equivalently, frequency reporting satisfies  $f/\omega=1/(2\pi)$ , matching the offset used in the main text and tested in the roadmap (Sec. C). This anchors the per-radian normalization directly to a standard boundary term (no model-specific assumptions beyond regularity).

# H Deterministic Simulation (Boundary-Curvature Sweep; verification only)

**Methods.** A deterministic sweep was carried out to verify the closed-form relations. Fractional perturbations in the outer circumference were applied,  $c_0 \to c_0(1+\delta)$  with  $\delta \in [-0.05, 0.05]$  in steps of 0.001, together with multiplicative rescalings of the bridging factor,  $C_f \in \{0.8, 0.9, 1.0, 1.1, 1.2\}$ . For each grid point, the curvature  $K = (8\pi/c_0)^2$ , cosmological constant  $\Lambda = \frac{7}{60} K C_f$ , and derived densities  $\rho_{\Lambda} = \Lambda c^2/(8\pi G)$ ,  $\epsilon_{\Lambda} = \Lambda c^4/(8\pi G)$  were computed in double precision. No stochastic elements or fit parameters enter. Outputs comprise a consolidated CSV grid and regression summaries.

Results. Figure 6 shows log-log regressions of  $\ln(\Lambda)$  against  $\ln(c_0)$  across the full sweep; fitted slopes are  $-2.000 \pm 0.002$  with  $R^2 > 0.9999$ , matching the analytic sensitivity  $\partial \Lambda/\partial c_0 = -2\Lambda/c_0$ . Figure 7 presents linear regressions of normalised  $\Lambda/L_0$  against the  $C_f$  scale at fixed  $c_0$  (with  $L_0$  the baseline at  $C_f = 1$ ); the fitted slope is  $1.000 \pm 0.001$  with intercept statistically indistinguishable from zero  $(R^2 \approx 1)$ .

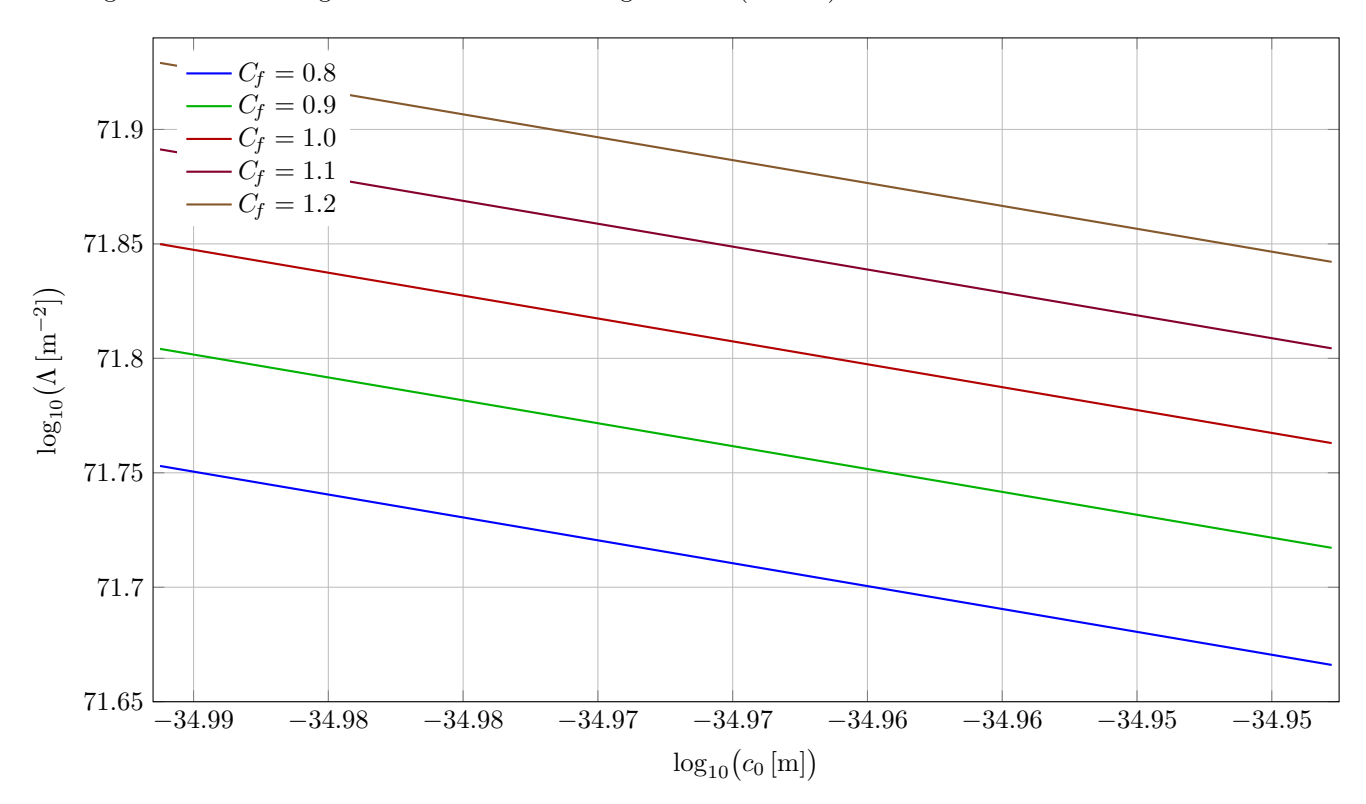


Figure 6: Log-log regressions of  $\ln(\Lambda)$ . Each coloured line corresponds to a different  $C_f$  value, and the fitted slopes are consistent with -2 ( $R^2 > 0.9999$ ).

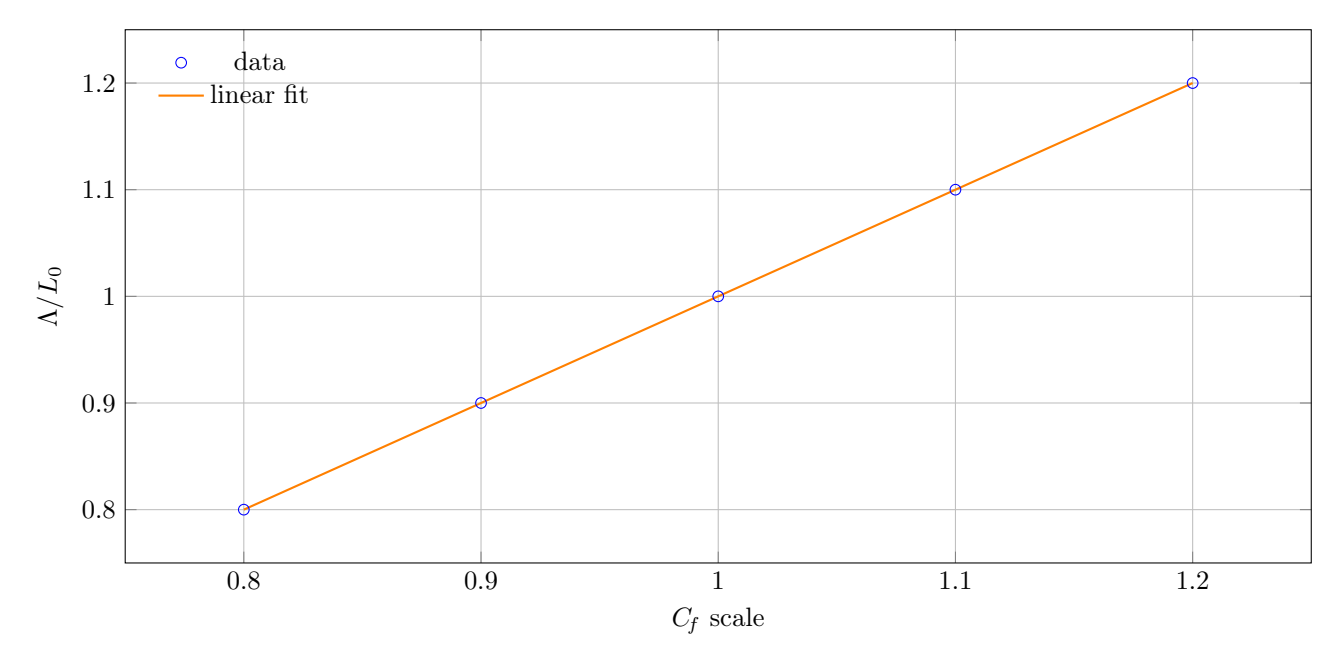


Figure 7: Linearity of  $\Lambda/L_0$  with  $C_f$  at baseline  $c_0$ . The fitted slope is  $1.000 \pm 0.001$  with an intercept statistically indistinguishable from zero and  $R^2 \approx 1$ .

Table 4: Counterfactual control: winding m > 1 injects an unconstrained integer into  $S_{\text{micro}} = k_B \ln(W^m)$ , breaking the canonical area-law match at fixed  $c_0$ .

$\overline{m}$	$S_{\text{micro}}/S_{\text{micro}}(m=1)$	Comment
1	1	Minimal closure (canonical match)
2	2	Integer injection (breaks canonical match)
3	3	Integer injection (breaks canonical match)

# Microphysical Derivation of $c_0$ (Full Details)

This appendix provides the full derivation of the entanglement–gravity crossover hypothesis outlined in Sec. 22. In 3+1D quantum field theory, the vacuum entanglement entropy across a smooth boundary obeys an area law  $S_{\rm ent} \sim \kappa_{\rm eff} A/\varepsilon^2$ , where  $\varepsilon = 1/k$  is a UV length cutoff and  $\kappa_{\rm eff}$  depends on the field content and spin statistics. The per-radian entanglement entropy reads

$$S_{\mathrm{ent}}^{(\mathrm{per\ rad})}(k) = \bar{\kappa}_{\mathrm{eff}} A k^2, \qquad \bar{\kappa}_{\mathrm{eff}} := \frac{\kappa_{\mathrm{eff}}}{2\pi},$$

while the Bekenstein-Hawking entropy on the circumference-based boundary  $A = \alpha \pi r_*^2$  with  $r_* = c_0/(8\pi)$  is

$$S_{\rm BH} = \frac{k_B c^3}{4G\hbar} A = \frac{k_B c^3}{4G\hbar} \alpha \pi \left(\frac{c_0}{8\pi}\right)^2.$$

Equating  $S_{\text{ent}}^{(\text{per rad})}(k_{\star})$  and  $S_{\text{BH}}$  and cancelling A yields

$$\bar{\kappa}_{\mathrm{eff}} k_{\star}^{2} = \frac{k_{B}c^{3}}{4\bar{\kappa}_{\mathrm{eff}}G\hbar}, \qquad \Rightarrow \qquad k_{\star} = \sqrt{\frac{k_{B}c^{3}}{4\bar{\kappa}_{\mathrm{eff}}G\hbar}}.$$

The microphysical circumference then follows as

$$c_0 := \frac{2\pi}{k_+} = 4\pi\sqrt{\bar{\kappa}_{\mathrm{eff}}}\,\ell_p,$$

where  $\ell_p = \sqrt{\hbar G/c^3}$  is the Planck length (restoring  $k_B$  rescales  $\bar{\kappa}_{\rm eff}$ ). Writing  $c_0 = \gamma \, \ell_p$  with  $\gamma := 4\pi \sqrt{\bar{\kappa}_{\rm eff}}$  and  $\bar{\kappa}_{\rm eff} := \kappa_{\rm eff}/(2\pi)$ , the predicted sum rule reads

$$\kappa_{\rm eff} = 2\pi \, \bar{\kappa}_{\rm eff} \approx 2\pi \left(\frac{\gamma}{4\pi}\right)^2 \approx 0.0176.$$

Hence

$$\bar{\kappa}_{\rm eff} pprox \left( rac{\gamma}{4\pi} 
ight)^2 pprox 2.80 imes 10^{-3}, \qquad \gamma = 4\pi \sqrt{\bar{\kappa}_{\rm eff}} pprox 0.665,$$

so that

$$c_0 = \gamma \, \ell_p \approx 0.665 \, \ell_p$$
.

This identifies a concrete quantum-field-theory sum rule:

$$\kappa_{\text{eff}} = \sum_{\text{SM species}} \left( N_s \, \kappa_s + N_f \, \kappa_f + N_v \, \kappa_v \right) \stackrel{!}{=} \frac{\gamma^2}{8\pi}$$

with  $\gamma := c_0/\ell_p \approx 0.665$ . The equality above states that the Standard Model entanglement coefficients must sum to the predicted  $\kappa_{\rm eff}$ . If they do, the UV crossover scale  $k_{\star}$  is fixed and  $(c_0 \approx 0.665 \, \ell_p)$  follows directly from microphysics, without cosmological input. No observational value of  $\Lambda$  enters this derivation; only  $(c, G, \hbar)$  and QFT coefficients are required. The value of  $c_0$  derived here reproduces the curvature scale  $r_h = c_0/(8\pi)$  used in Sec. 6.

# Acknowledgments

The author gratefully acknowledges the foundational work in differential geometry, geometric quantisation, and gravitational thermodynamics that underpins this analysis. Developments in boundary terms, entropy formulations, and topological quantisation have provided essential tools for the formulation of the toroidal framework and the derivation of the cosmological constant. The literature connecting holography, entanglement entropy, and gravitational dynamics has also shaped the construction and positioning of this approach.

#### REFERENCES

- P. Collaboration et al., Astronomy and Astrophysics 641, A6 (2020).
- D. Collaboration et al., Journal of Cosmology and Astroparticle Physics 2025, 021 (2025).
- A. Collaboration et al., Astrophysical Journal 962 (2024), 10.3847/1538-4357/acff5f.
- A. Einstein, Sitzungsberichte der Koeniglich Preussischen Akademie der Wissenschaften, 142 (1917).
- H. Fritzsch, Vom Urknall zum Zerfall der Sterne (Deutscher Taschenbuch Verlag, Munich, 1984).
- P. Jordan, Schwerkraft und Weltall (Vieweg, Braunschweig, 1955).
- E. P. Verlinde, Journal of High Energy Physics 2011, 29 (2011).
- T. Padmanabhan, Reports on Progress in Physics 73, 046901 (2010).
- J. D. Bekenstein, Physical Review D 7, 2333 (1973).
- S. W. Hawking, Communications in Mathematical Physics 43, 199 (1975).
- S. Weinberg, Reviews of Modern Physics 61, 1 (1989).
- A. Padilla, "Lectures on the cosmological constant problem," (2015), arXiv:1502.05296.
- E. J. Copeland, M. Sami, and S. Tsujikawa, International Journal of Modern Physics D 15, 1753 (2006).
- A. G. Cohen, D. B. Kaplan, and A. E. Nelson, Physical Review Letters 82, 4971 (1999).
- M. Li, Physics Letters B 603, 1 (2004).
- S. Wang, Y. Wang, and M. Li, Physics Reports 696, 1 (2017).
- T. N. Li, Y. H. Li, G. H. Du, P. J. Wu, L. Feng, J. F. Zhang, and X. Zhang, European Physical Journal C 85, 608 (2025).
- A. Samaddar et al., Physics of the Dark Universe 44, 101489 (2024).
- G. G. Luciano, A. Paliathanasis, and E. N. Saridakis, Journal of High Energy Astrophysics 49, 100427 (2025).
- G. B. Bianconi, Physical Review D 111, 066001 (2025).
- A. Alonso-Serrano and M. Liska, Physical Review D 111, 064019 (2025).
- V. M. Tikhomirov, Stories About Maxima and Minima (American Mathematical Society, Providence, RI, 1990).
- R. M. Wald, Physical Review D 48, R3427 (1993).
- V. Iyer and R. M. Wald, Physical Review D 50, 846 (1994).
- T. Jacobson, Physical Review Letters 75, 1260 (1995).
- T. Faulkner, A. Lewkowycz, and J. Maldacena, Journal of High Energy Physics 2013, 74 (2013).
- N. Lashkari, M. B. McDermott, and M. Van Raamsdonk, Journal of High Energy Physics 2014, 195 (2014).
- S. Ryu and T. Takayanagi, Physical Review Letters 96, 181602 (2006).
- V. E. Hubeny, M. Rangamani, and T. Takayanagi, Journal of High Energy Physics 2007, 062 (2007).
- T. M. Davis, in Encyclopedia of Astrophysics, edited by I. Mandel (Springer, 2026) Chap. 1, pp. 1–16, section editor: Cullan Howlett, arXiv:2509.09954 [astro-ph.CO] .
- S. M. Carroll, Living Reviews in Relativity 4, 1 (2001).